INVESTIGATION
OF A MICROMETEOROID VEHICLE DAMAGE
ASSESSMENT SYSTEM

SUMMARY REPORT
November 19, 1962

Prepared For

THE NATIONAL AERONAUTICS AND SPACE ADMINISTRATION

George C. Marshall Space Flight Center

Huntsville, Alabama

Authors:
W. C. Cooley
P. G. Luckhardt

Prepared By

EXOTECH INCORPORATED
4208 Wheeler Avenue
Alexandria, Virginia

OTS PRICE

TABLE OF CONTENTS

Table of Contents (continued)

LIST OF ILLUSTRATIONS

List of Illustrations (continued)

LIST OF TABLES

1 SUMMARY

Experimental and analytical studies have been conducted leading to design specifications for micrometeoroid penetration detection systems based on the detection of infrared or visible radiation inside a space vehicle. Micrometeoroid impact simulation was achieved in a hypervelocity facility utilizing a powder gun and producing impact velocities in excess of 7500 feet per second. Analytical studies were conducted to determine the optimum design for optical and sensor systems for use in space vehicle propellant tanks. The analysis of sensor requirements included theoretical and experimental studies of the characteristics of infrared. and visible radiation produced behind a wall by penetrating impacts.

The studies indicate that effective detection of micrometeoroid penetration through propellant tank walls may be achieved by the use of infrared sensitive detection systems. Performance and cost considerations dictate the use of lead sulfide photoconductive sensors of sufficient surface area to provide requisite optical collecting surface without the use of optical reflective or refractive elements. Amplification and readout of the detected signals may utilize conventional electronic practice consistent with the detection sensitivity required for any particular application. Design specifications are included for a system that should be able to detect a penetration that results in a 20 mil diameter hole in a propellant tank wall at a range of approximately 30 feet, assuming negligible absorption of radiation by the propellant.

II INTRODUCTION

The meteoroid hazard to space flight has been the subject of considerable investigation and is undergoing continuing study (References 1, 2, and 3). The hazards include those of direct damage to structures and crew members, and creation of leaks through which fuels, oxidizers, gaseous atmosphere or other fluids may be lost. It is therefore desirable to obtain data on the frequency and extent of meteoroid penetrations during the time of flight of a vehicle in order to provide a warning that leakage will occur and also to accumulate data on meteoroid population to aid in the design of future vehicles. The objective of this study is the determination of feasibility of various sensing system concepts, leading to system design specifications for a laboratory model.

Numerous investigations have been performed of the characteristics of hypervelocity impact (References 1, 4, and 5). These have included experimental and theoretical studies of projectile ablation, crater formation and related effects. However, current literature appears to be lacking in conclusive data on the thermal or radiative characteristics of material driven through wall structures by penetrating impact at hypervelocities. Several mathematical correlations have been postulated for the relationships between crater diameter and measurable characteristics of the impacting particle. However, the mechanism and extent of conversion of particle kinetic energy to thermal internal energy of the products of penetration has not been conclusively resolved. Also, the available data concerning impacts between dissimilar materials is fragmentary.

Considerable work has been done in development of practical infrared detection systems, to the extent that the system requirements of a meteoroid penetration

detector may be adequately fulfilled within the current state of the art, once the intensity, spectral distribution and time variation of the incident radiation is known.

The overall approach followed in this study included experimental evaluation of sensor performance in detecting penetrations, review of available literature covering transmission of electromagnetic radiation through various propellant fluids, and analysis of the optical, sensor, and electronic requirements of the system. The experimental study was conducted in a hypervelocity facility developed by Exotech, in which hypervelocity impacts are achieved with controlled variations in impact particle size, target thickness, and composition of the atmosphere into which penetration occurs. The literature search of transmission characteristics was undertaken to determine whether absorption of radiation by propellant fluids within a fuel tank would interfere excessively with detection of infrared or visible radiation. The theoretical analysis was directed toward optimizing the design of the required components under various assumed operating situations.

Geometrical optical analysis was conducted to determine the optimum optical system design for cylindrical or semi-cylindrical tanks. Selection of a lead sulfide sensitive element was based upon existing information on spectral range, detectivity, cost, reliability, and general system compatibility as compared with alternative materials. The selection of lead sulfide was verified by the experimental program. An analysis of the electronic sub-system design requirements was conducted. A general description of the required amplifier and readout characteristics is included, but detailed design of these circuits is not possible without additional knowledge of the characteristics of the overall electronic system in which the detection system will be placed, in particular the pulse voltage required to operate the memory and readout system.

III EXPERIMENTAL PROCEDURE AND RESULTS

A.   Overall Construction of Micrometeoroid Simulator

For conducting hypervelocity impact tests, the hypervelocity facility shown in Figures 1 and 2, was used. Steel balls of various sizes were mounted on the front of nylon sabots, which in turn were loaded into cartridges for a 220 Swift rifle. The cartridges were charged with 25 grains of Hercules unique powder, and were fired from the rifle through a two feet diameter by five feet long vacuum tank, as shown in the photographs. Upon firing, the sabot and steel ball traveled together through the vacuum tank to a sabot deflector assembly. Within this assembly, the sabot was deflected from the initial path by a steel plate, while the steel ball, which had been mounted at the center of the cross-section of the sabot, was left free to travel in its original direction. The steel ball then continued through a connecting tube which terminated inside a vertically aligned receiver tank. The end of the tube was closed with a threaded fitting to hold various thicknesses of flat circular aluminum alloy diaphragms which sealed the vacuum system and served as targets for the impacting balls. Penetration of the steel balls through these diaphragms was the phenomenon that was observed in the experimental phase of this study. Within the receiver tank a thermally insulated steel container was situated to accommodate various sensor elements (infrared and visible). The steel container was equipped to hold and discharge cryogenic liquids, or gases other than air, at approximately atmospheric pressure. This design permitted study of the penetration phenomena with the sensors immersed in various controlled environments.

A Welch Duo-Seal mechanical vacuum pump (15 CFM) was connected through galvanized pipe and vacuum hose to the vacuum tank of the simulator. The structure was made leak-tight from the breach of the rifle to the diaphragm, so that a pressure below 1 Torr could be maintained after a pump-down time of approximately
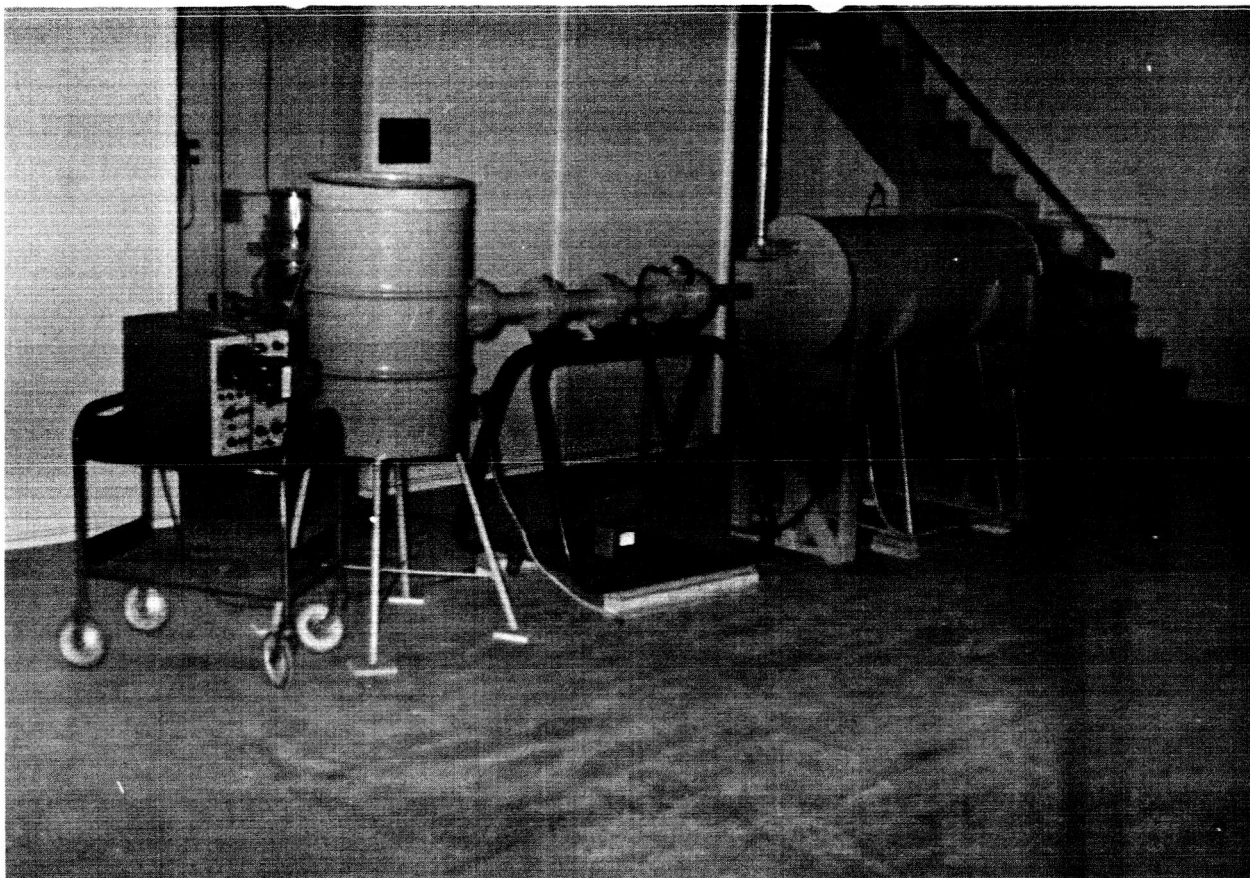
MICROMETEOROID SIMULATOR

FIGURE 1
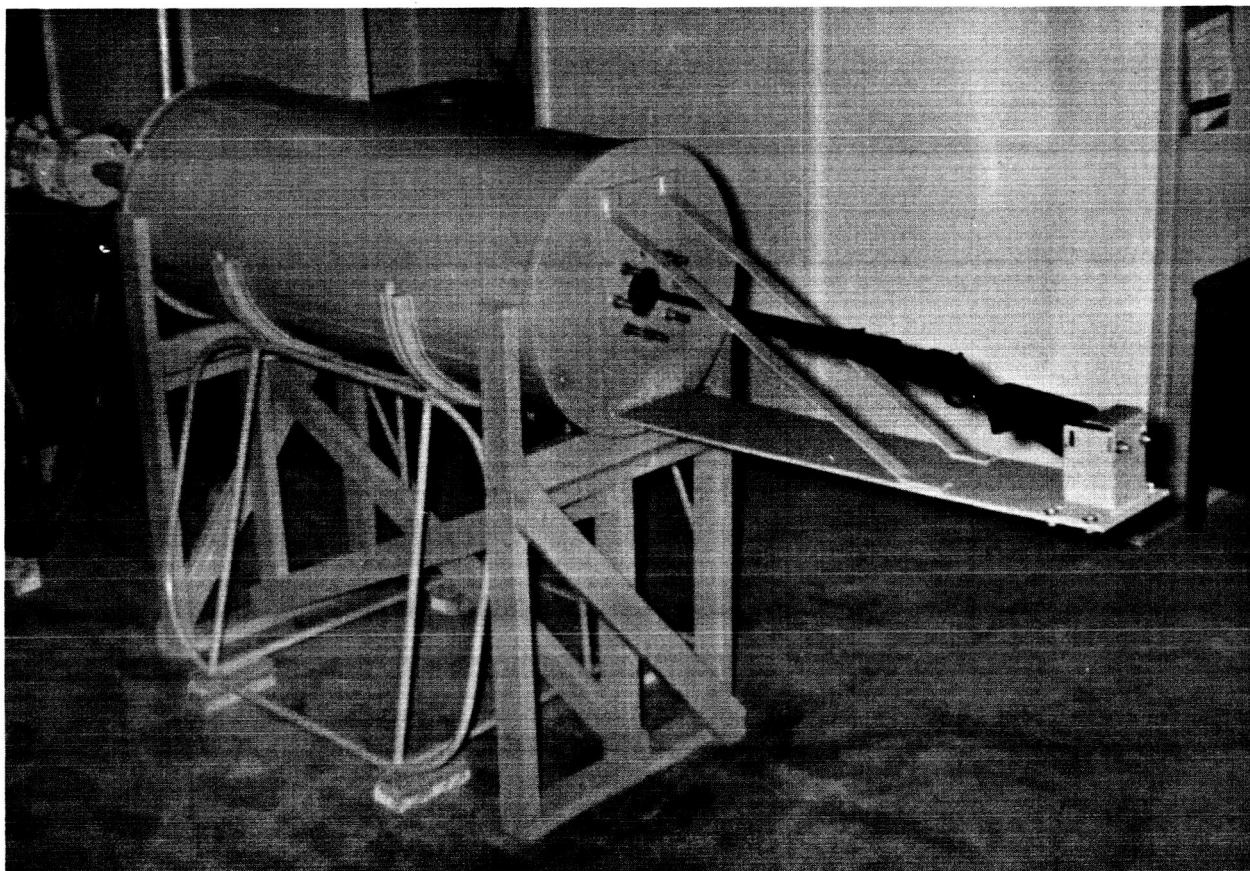
RIFLE AND VACUUM TANK

Figure 2

10 minutes. The velocities of the steel ball before impact were observed to be 7500 feet per second, plus or minus 10 percent. Stainless steel balls of selected diameter ranging from 0.015 inch through 0.062 inch were used during the tests.

B.   Instrumentation

During the conduct of the tests two sensing systems were employed, the first using a lead sulfide photoconductive sensor and the second using a silicon photovoltaic cell. For calibration purposes, these systems were tested with separate calibration apparatus, in which the temperature and surface area of radiating objects could be controlled.

1. Infrared Sensitive System

Lead sulfide photoconductive sensors with various values of impedance and sensitive area were obtained from Infrared Industries, Inc., Waltham, Mass. Preliminary calibration tests were conducted with the sensors mounted at the focal point of infrared reflective parabolic mirrors, which provided appreciable optical gain to the overall detector system. However, as is discussed in a following section, design studies indicated the desirability of using a relatively large area sensor of intermediate impedance, without any associated optical collecting elements. Accordingly, the majority of the penetration detection tests were conducted with a sensor of 50 kilohms resistance having a sensitive surface area of 0.005 square inch, and an interdigital electrode configuration without additional optical collecting elements. The sensor was biased by a DC potential of 22.5 volts and the sensor output was fed directly into one channel of a Tektronix #531 oscilloscope, without pre-amplification. The circuit is shown in Figure 3.

INFRARED SENSOR CIRCUIT

FIGURE 3
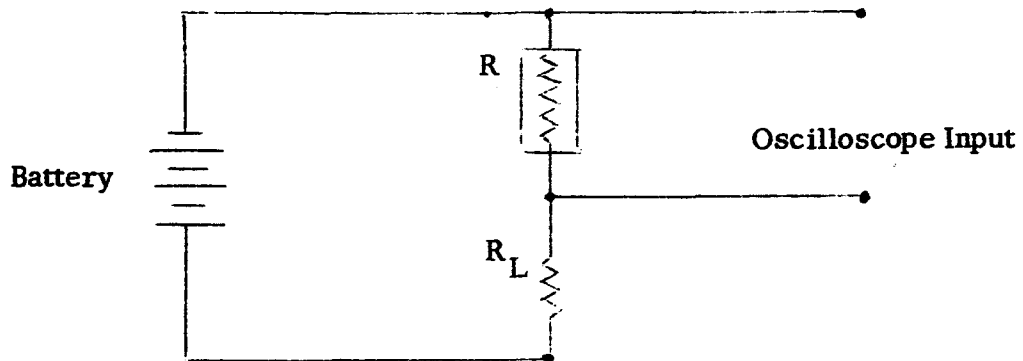
R   =   Resistance of Infrared Sensor, 50 kilohms (dark resistance)

R_L =   Matching load resistance, 47 kilohms

The infrared sensor was mounted in the receiver tank to view the back side of the aluminum disphragm at the time of impact. The sensor was mounted at a distance of approximately three inches back of the diaphragm with its surface parallel to the line of fire and at a distance of three inches from the central axis of the diaphragm. This arrangement gave a view angle of 45 degrees for a penetration at the center of the diaphragm.

2. Visible Sensitive System

Silicon photovoltaic sensors were mounted in the receiver tank and used simultaneously with the infrared sensor. The silicon sensors were Hoffman Electronic Corporation, Type No. 110   solar cells having a sensitive surface area of 0.14 square inches. These sensors were connected directly into the second channel of the Tektronix . #531 oscilloscope.

Permanent records of the signals generated by the sensors as a result of impacts were obtained through the use of a Polaroid camera mounted on the oscilloscope, with the shutter manually opened immediately before firing and closed immediately after impact. The camera was a Fairchild Camera and Instrument Corporation Model 196, with Polaroid Type 42 film used throughout the tests.

The oscilloscope sweep was triggered by a crystal vibration sensor (barium titanate) mounted on the breach of the rifle. Upon firing, an electrical signal was generated in this sensor, and was fed into the external trigger circuit of the oscilloscope.

3. Velocity Measurement

For measurements of velocity of the steel ball before impact, a visible sensor (Hoffman 110 C) was mounted at a transparent window in the front wall of the vacuum tank, to be responsive to the visible flash at the muzzle of the rifle coincident with exit of the sabot. An infrared sensor was mounted in its customary place in the receiver tank. As the gun was fired, the oscilloscope traces for both sensors were triggered by the impulse from the barium titanate sensor. As the sabot left the muzzle, the visible sensor generated a signal causing a sharp vertical deflection of its trace. Finally, when the steel ball penetrated the diaphragm, the signal from the infrared sensor caused a vertical deflection of its trace. Thus, the elapsed time of travel from the gun muzzle to impact at the diaphragm was measured by noting on the photograph the distance between the vertical deflections for the visible and infrared sensor, and noting the sweep rate of the oscilloscope. In Figure 4, the upper trace is that from the visible sensor at the gun muzzle while the lower trace is that from the infrared sensor at the diaphragm. The measured distance between the muzzle and the diaphragm is 102 inches, and the sweep speed of the oscilloscope was set at 0.5 ms/cm. The distance between vertical deflections of the two pulses is 2.3 cm, which is therefore equivalent to 1.15 ms. The velocity of the ball is then the distance

traveled divided by the elapsed time, or:

$$V = \frac{102}{12\,(1.15)\,(10)^{-3}} = 7400 \text{ ft/sec}$$

Additional observations indicated that all velocities were within the range of 7500 feet per second plus or minus 10 percent.

PROJECTILE VELOCITY MEASUREMENT
FIGURE 4
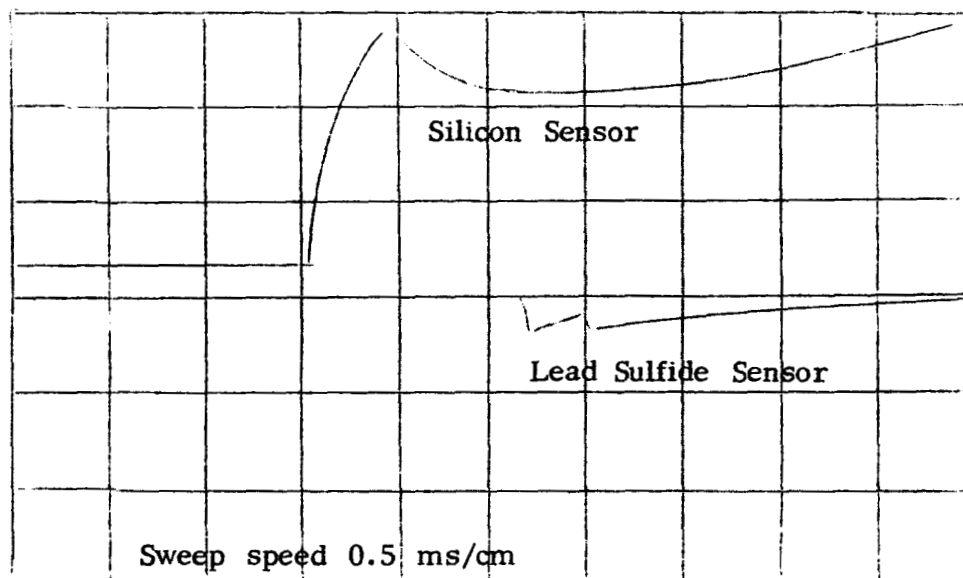
4. Vacuum Measurement in the Meteoroid Simulator

Measurements of the vacuum in the simulator were made with a mercury U-tube manometer, with measurements taken at each firing. Values of barometric pressure were used to determine the absolute tank pressure. Pressures of approximately 1 mm Hg or less were attained prior to each test. The pressure increase caused by firing the rifle was of the order of one mm Hg.

- 9 -

5. Calibration Procedure

To obtain reference data for evaluating sensor performance in the actual firings, the sensors were mounted at various positions in front of a vertical drop tube. Metal particles of known composition and surface area were heated to selected temperatures in the range from 525 degrees F. to 1010 degrees F. and dropped through the tube for a known vertical distance of free fall of either 72 inches or 90 inches. Thus, radiant sources of predictable radiant power were dropped at known average velocities through the fields of view of the sensors. The resultant photographs of signal traces served as reference data for comparison with signals generated in the penetration tests.

A Chromel-Alumel thermocouple pyrometer (Temco, Portable Indicating) was used for measurements of the particle temperature prior to each drop. The particles included copper-coated "BB's" with a mean diameter of 0.173 inch, and short aluminum cylinders of various lengths and diameters.

C. Results

In presentation of results, the calibration data are tabulated in Table I, and the simulator test data are tabulated in Table II. A discussion of particular data points is included in later sections. Interrelationships of significant test variables are presented graphically in Figure 5 and in Figure 6. Figure 5 shows the variations in signal amplitude with variations in steel ball diameter for penetrating impacts, with the ratio of ball diameter to plate thickness held within the range from 3.20 to 4.00. Figure 6 shows the variation in signal amplitude with variation in oxygen content of the receiver tank for constant impact conditions.

TABLE I

TABULATION OF CALIBRATION DATA

Designation	Sensor		Optical Collecting Elements		Radiation Source					Signal		Sensor (orientation)	
	Material	Nominal Active Area (in^2)	Type	Surface Area (in^2)	Type	Surface Area (in^2)	Temperature ($^\circ$F)	Distance to Sensor (inches)	Angle of Incidence ($^\circ$)	Amplitude (volts)	Form (No. of peaks)	Perp.	Para.
C-101	PbS	0.0006	Paraboloid	6	CuO-BB	0.094	580	6.5	0	0.09	double	x	
C-102	PbS	0.0006	"	6	"	0.094	580	6.5	9	0.05	single	x	
C-103	PbS	0.0006	"	6	"	0.094	580	6.5	0	0.10	double		x
C-104	PbS	0.0006	"	6	"	0.094	580	6.5	9	0.02	single		x
C-105	PbS	0.0006	"	6	"	0.094	580	13	0	0.09	double	x	
C-106	PbS	0.0006	"	6	"	0.094	580	13	0	0.09	single		x
C-107	PbS	0.0006	"	6	"	0.094	525	6.5	0	0.02	double	x	
C-108	PbS	0.0006	"	6	"	0.094	525	6.5	0	0.02	double		x
C-120	PbS	0.005	None	-	"	0.094	1010	3	0	2.05	single		
C-121	PbS	0.005	"	-	"	0.094	900	3	0	0.70	"		
C-122	PbS	0.005	"	-	"	0.094	800	3	0	0.25	"		
C-123	PbS	0.005	"	-	"	0.094	850	3	0	0.50	"		
C-124	PbS	0.005	"	-	"	0.094	700	3	0	0.10	"		
C-125	PbS	0.005	"	-	Al Cyl	0.190	800	3	0	0.39	"		
C-126	PbS	0.005	"	-	"	0.190	950	3	0	1.15	"		
C-127	PbS	0.005	"	-	"	0.190	1010	3	0	1.25	"		
C-128	PbS	0.005	"	-	"	0.190	700	3	0	0.12	"		
C-129	PbS	0.005	"	-	"	0.095	980	3	0	0.19	"		
Silicon*	0.14												

* No signals were detectable from the silicon sensor from hot particles dropped through the drop tube.

- 11 -

TABLE II
TABULATION OF TEST DATA

Desig-nation	IMPACT					PbS SENSOR			Si SENSOR(.14in²) SIGNAL		SENSOR*ORIENTATION		REMARKS
	Steel Ball Diam. (d in.)	Al.Diaphragm thickn. (T in.)	Ratio d/T	Penetration hole diam. (inches)	Nominal Active Area (in²)	Area optical collecting elem (in²)	Signal Amplitude (volts)	Signal Form (No.of peaks)	Amplitude (volts)	Form (No.of peaks)	Side by Side	Front to Front	
T-101	0.030	0.063	4.77	0.070	0.0006	6	0.23	single	0	-			Si cell used for triggrg.
T-102	0.030	0.063	4.77	0.064	0.0006	6	0.18	single	0	-			Si cell used for triggrg.
T-201	0.025	0.063	3.98	0.050	0.005	-	0.5	single	N/A	-			Si cell at muzzle
T-202	0.025	0.063	3.98	0.050	0.005	-	0.4	double	N/A	-			Si cell at muzzle
T-203	0.015	0.040	3.75	0.029	0.005	-	0.08	single	N/A	-			Si cell at muzzle
T-204	0.015	0.040	3.75	0.029	0.005	-	0.18	double	N/A	-			Si cell at muzzle
T-301	0.062	0.156	3.98	0.125	0.005	-	8.5	single	0.30	double			Air
T-302	0.062	0.156	3.98	0.130	0.005	-	13.5	single	0.20	double		x	"
T-303	0.062	0.125**	N/A	0.125	0.005	-	1.5	single	0.01	single		x	"
T-304	0.062	0.156	3.98	0.120	0.005	-	11.5	single	0.11	double		x	"
T-305	0.062	0.156	3.98	0.120	0.005	-	22.0	double	0.20	double	x		Same as T-304 but in O₂
T-306	0.062	0.156	3.98	0.130	0.005	-	9.5	single	0.07	double	x		Same as T-304 but in He
T-307	0.062	0.090	6.90	0.120***	0.005	-	0	-	0.02	single	x		Sensors in LN₂
T-308	0.040	0.125	3.20	0.045	0.005	-	2.0	single	0.01	single	x		
T-309	0.040	0.090	4.44	0.085	0.005	-	5.0	double	0.025	single	x		
T-401	0.062	0.250	N/A	#	0.005	-	0	-	0	-			
T-451	N/A	0.250	N/A	0.125##	0.005	-	0	-	0	-			
T-452	N/A	0.250	N/A	0.125##	0.005	-	0	-	0	-			

* All sensors placed at radial distance of 3 inches from axis of diaphragm. However, the precise point of impact on the diaphragm is not controllable. Thus, the optical line of travel of the penetration products **varied** somewhat from a 3-inch distance to the sensor.

** Insulated Section - Saturn S-IV tank wall

***Smaller Hole size may be due to lower temperature of aluminum diaphragm

\# Non-penetrating impact: 0.130 inch diameter; 0.195 inch depth

\#\# No ball fired. No muzzle flash detected through drilled hole in diaphragm
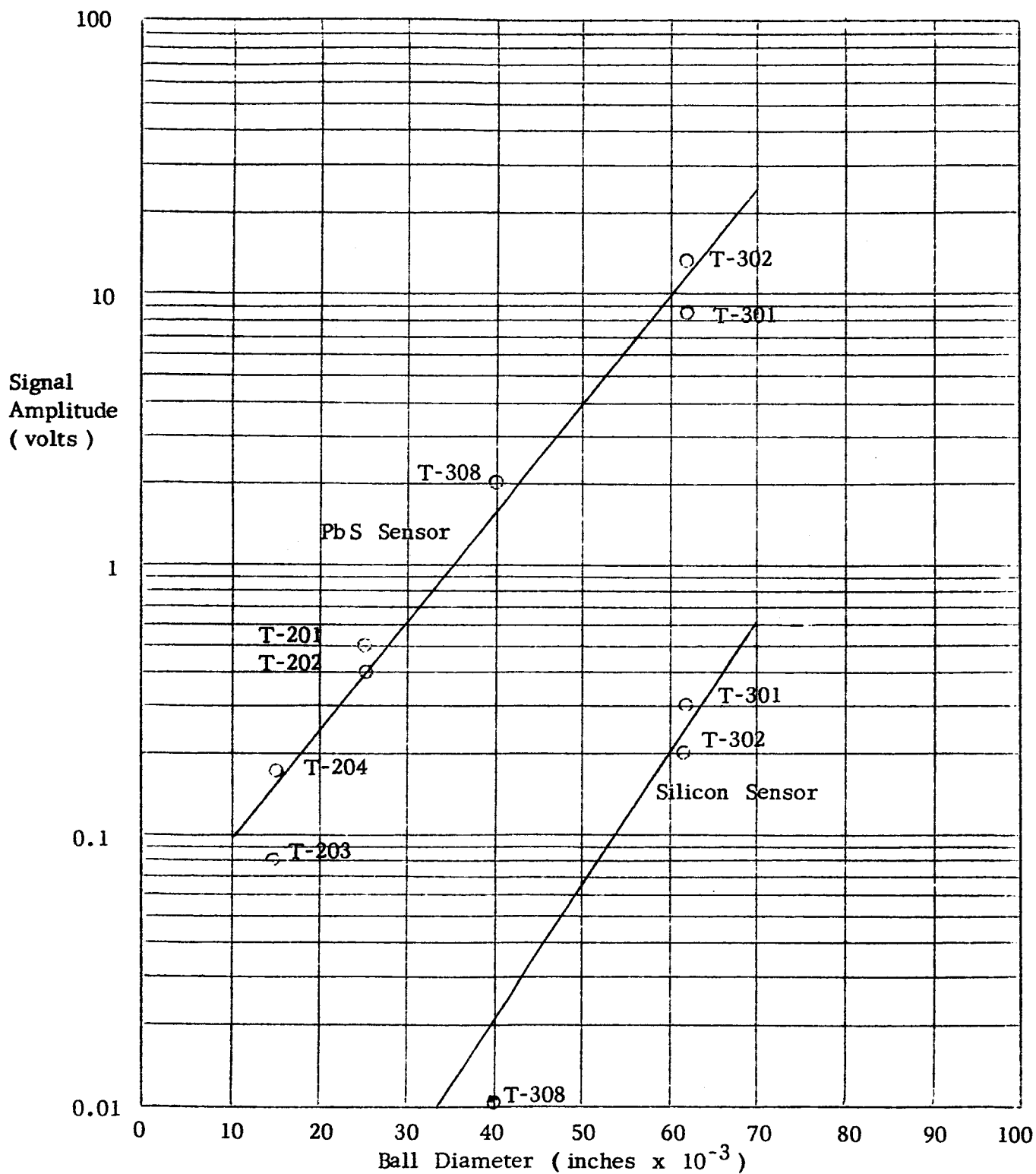
VARIATION OF SIGNAL AMPLITUDE WITH BALL SIZE

FIGURE 5

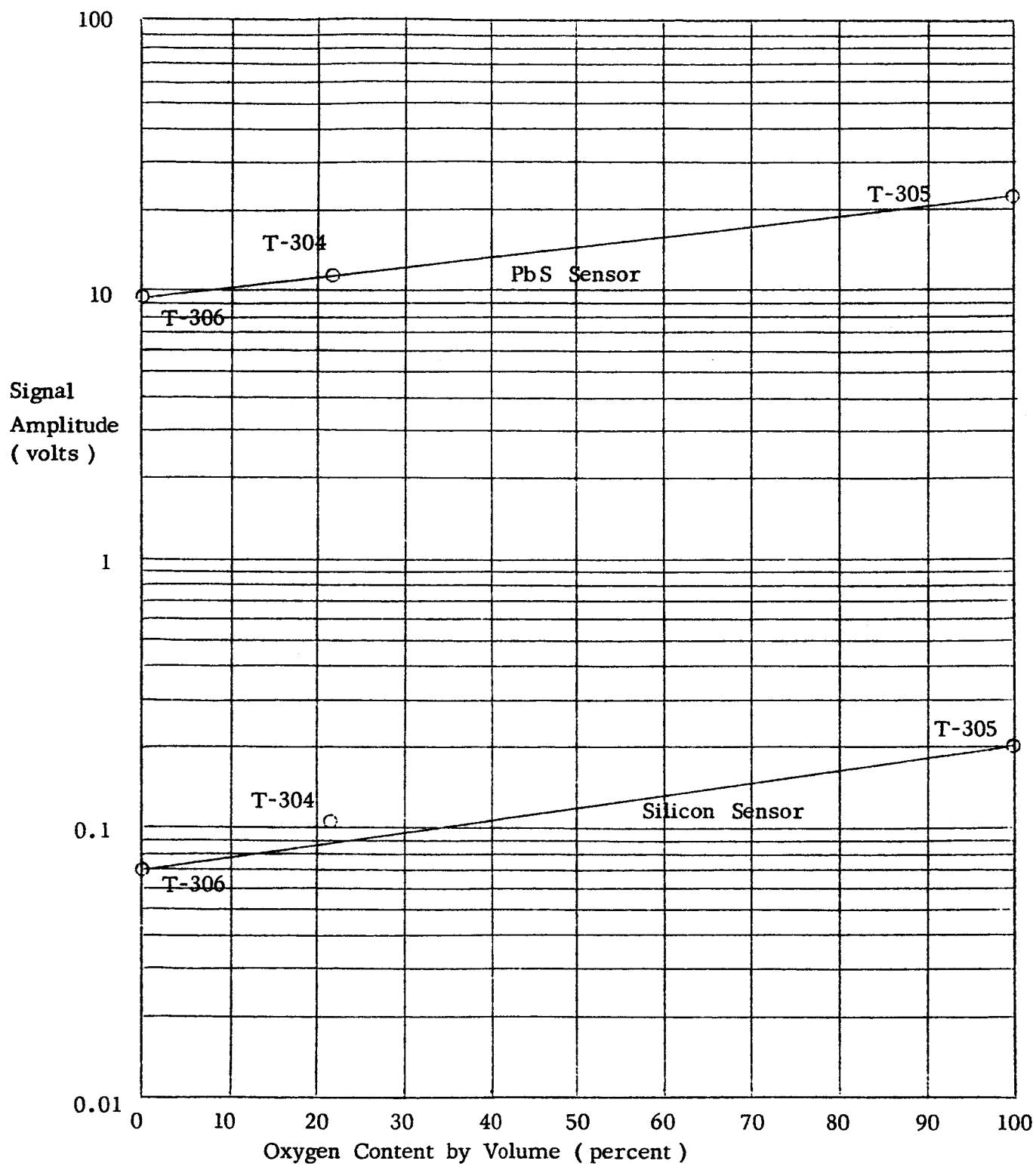VARIATION IN SIGNAL AMPLITUDE WITH OXYGEN CONTENT

FIGURE 6

Discussion of Results

Qualitatively, the test results may be stated as follows:

1. For the simulated conditions, lead sulfide sensor systems provide very
    effective means for detecting penetrating (i.e. puncturing) impacts by
    simulated meteoroids (see Figure 5).

2. The effectiveness of visible (silicon) photovoltaic sensor appears limited
    for detection of impacts of the simulated meteoroids. The observed signal
    voltages from the silicon sensors were invariably much lower than those
    from the PbS sensors.

3. Non-penetrating (i.e., non-puncturing) impacts were not detectible by
    either infrared or visible sensor systems on the inside of the receiver tank
    because no spallation was produced from the rear face of the aluminum
    diaphragms by non-penetrating impacts. Therefore, non-penetrating im-
    pacts would not cause the sensor to generate signals that might be indis-
    tinguishable from those caused by penetration (T-401).

4. The environment into which the products of penetration (i.e. ejected
    diaphragm material plus any residue from the impacting particle) are
    emitted has a significant effect upon the amplitude of signals from the
    infrared sensor. Chemical oxidation reactions appear to occur when the
    penetration products pass through oxidizing atmospheres (Air, O_2) as
    inferred from larger signal amplitudes than observed when firing into
    inert gas (helium) (see Figure 6).

5. Performance of the PbS or silicon sensors is not impaired by operation
    within cryogenic liquids. The one data point (T-307 in Table II),
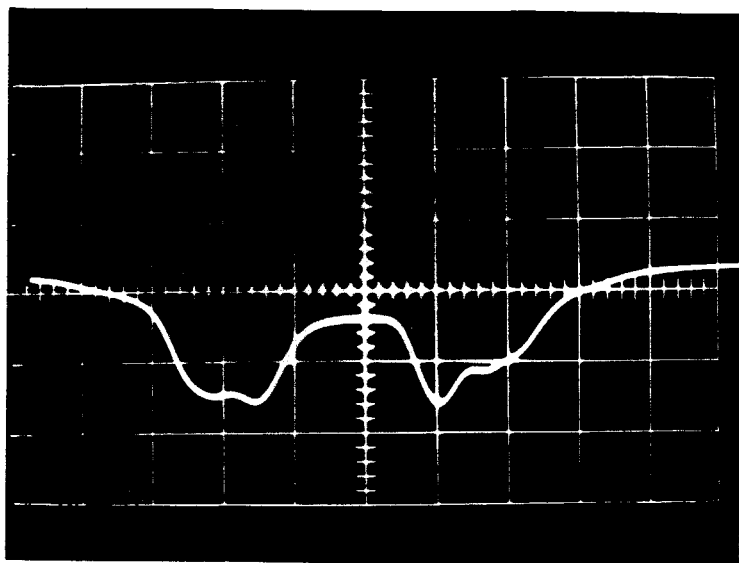
Figure 7 (a)
Calibration - With Mirror (C-103):
Trace from PbS Cell (0.05 v/cm)
Sweep - 0.5 ms/cm

Figure 7 (b)
Calibration - Without Mirror (C-120):
Upper Trace - Silicon Cell (0.05 v/cm)
Lower Trace - PbS Cell (1.0 v/cm)
Sweep - 0.5 ms/cm

16

Figure 8 (a)
Test Firing (T-301):
Dual Peak Waveform - Silicon Cell (0.2 v/cm)
Dual Peak Waveform - PbS Cell (5.0 v/cm)
Sweep - 0.5 ms/cm

Figure 8 (b)
Test Firing (T-308):
Upper Trace - Silicon Cell (0.05 v/cm)
Lower Trace - PbS Cell (5.0 v/cm)
Sweep - 0.5 ms/cm

Figure 9a
Firing into Saturn S-IV Wall Section (T-303):
Upper Trace - Silicon Cell (0.2 v/cm)
Lower Trace - PbS Cell (5.0 v/cm)
Sweep - 0.5 ms/cm

17
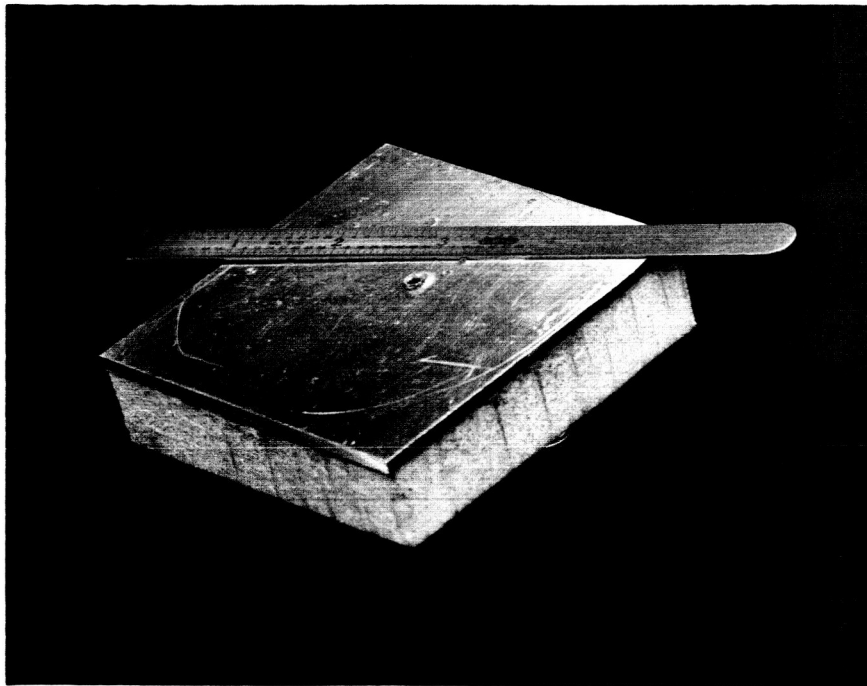
Figure 9 (b)
Penetration into Insulated
Section of Saturn S-IV Wall,
0.062 inch diameter Steel
Ball Fired at 7500 ft/sec

Front View
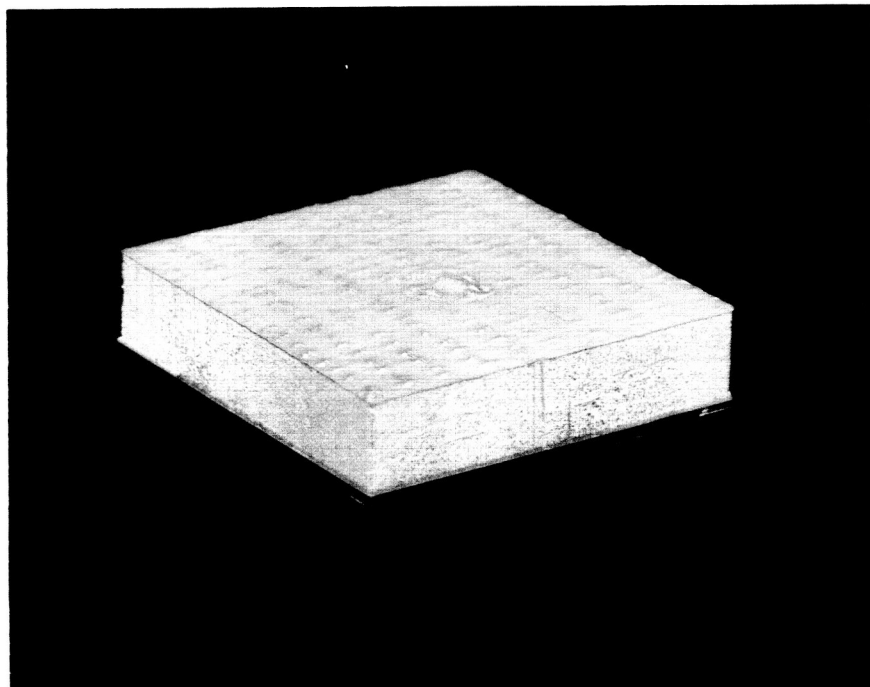
Figure 9 (c)
Penetration into Insulated
Section of Saturn S-IV Wall,
0.062 inch diameter Steel
Ball Fired at 7500 ft/sec

Rear View
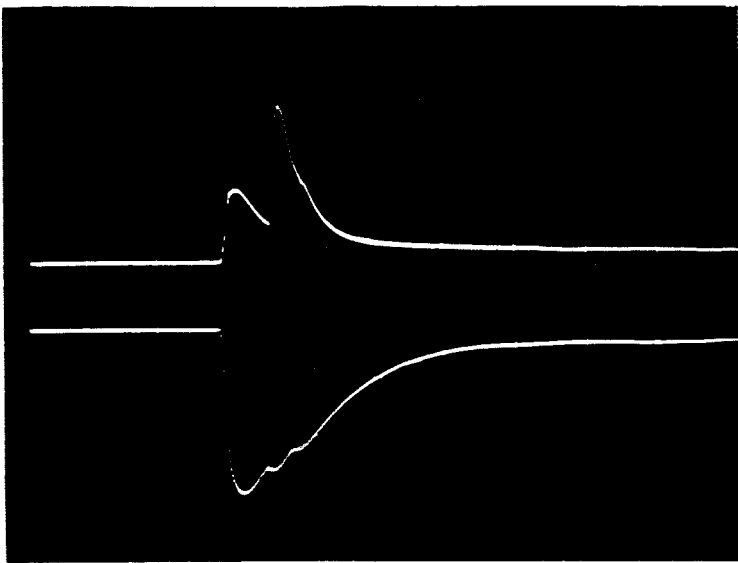
Figure 10 (a)
Firing into Air (T-304):
Upper Trace - Silicon Cell (0.05 v/cm)
Lower Trace - PbS Cell (5.0 v/cm)
Sweep - 0.5 ms/cm
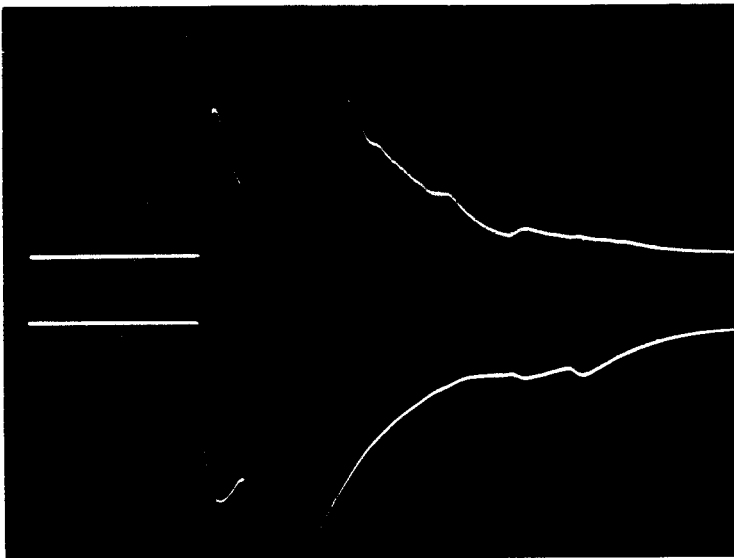
Figure 10 (b)
Firing into Gaseous Oxygen (T-305):
Upper Trace - Silicon Cell (0.05 v/cm)
Lower Trace - PbS Cell (5.0 v/cm)
Sweep - 0.5 ms/cm
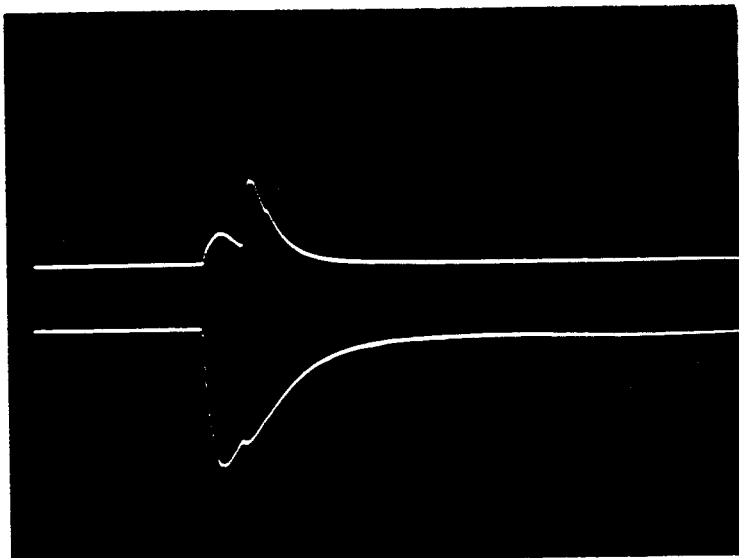
Figure 10 (c)
Firing into Gaseous Helium (T-306):
Upper Trace - Silicon Cell (0.05 v/cm)
Lower Trace - PbS Cell (5.0 v/cm)
Sweep - 0.5 ms/cm

obtained for a firing with liquid nitrogen in the receiver tank (covering both diaphragm and the sensors), does not show a discernible infrared signal. However, for this firing the gain adjustment on the oscilloscope for the infrared channel had been set at a very low level (10 v/cm), in anticipation that several shots would be required to determine the proper gain adjustment. However, before any additional penetration shots were attained, a leak developed in the receiver tank, requiring shutdown. It is believed that the low gain setting accounts for the absence of a discernible infrared signal. Both sensors were found to be in good working order when exposed to incandescent radiation sources after removal from the receiver tank.

Typical waveforms and diaphragm penetrations observed for various calibration and test conditions are indicated in Figure 7 through 10. It should be noted in the waveforms that a characteristic of the lead sulfide cells observed under controlled conditions, is a slower decay than rise of signal. Also, the second peak of the double peak signals observed in most of the penetration experiments is attributable to emission of radiation from impact of the penetration products on the rear wall of the receiver tank. In Figure 8 (a) for the double peaks of the visible sensor trace, the distance between the start of rise of each peak could result from an impact of penetration products traveling from the diaphragm to the rear wall of the receiver tank with a velocity of approximately 1600 feet per second. In some cases (see Figure 8 (b), the second peak was avoided by locating an optical shield so that it prevented the sensor from viewing the point on the rear wall of the tank at which the penetration products made impact. Figures 9 (b) and 9 (c) show the results of penetrating impact into the insulated section of the Saturn S-IV wall. The hole shown in the aluminum plate in Figure 9 (b) is typical of those observed for all penetrating impacts.

IV THEORETICAL DESIGN CONSIDERATIONS

This section discusses theoretical considerations that apply to the detection system design including the generation of electromagnetic radiation at the point of impact, the optical sensor element, and the electronic system design. The objective of the detection system is to detect the occurrence of penetration by micrometeoroids. Additional knowledge of the impact phenomenon is required in order that the detection system provide information on the location and hole size of penetrations. A discussion of the problems and solutions to hole size determination are included in Appendix A.

The objectives of this study have been the determination of feasibility and the specification of major design parameters for a detection system based upon the sensing of infrared and visible electromagnetic radiation generated by meteoroid penetrations through wall structures. The design of such a system must take cognizance of the various physical effects occurring in the generation, transmission, sensing and interpretation of the radiation phenomena occurring at impact. In terms of the system design, this includes consideration of the optics of the transmission and collection of the radiant energy from the source to the sensing element, the response characteristics of the sensing element, and the amplification and output characteristics of the electronic amplifying, data storage and readout sub-systems associated with the sensing element. This section discusses each of these areas in the following order:

A. Source Characteristics

B. Optics

C. Sensor Characteristics

D. Electronics.

A.   Source Characteristics

The emission of electromagnetic radiation from warm objectis has been studied in considerable detail, and a fundamental expression for the total radiant power emitted per unit area is given by the Stefan-Boltzmann Law:

$$R = \epsilon \sigma T^4 \tag{1}$$

where

R = Total radiant flux emitted per unit area (Radiance)

ϵ = Emissivity (black body = 1)

σ = Stefan-Boltzmann Constant (5.6686×10^{-12} watts cm^{-2} deg^{-4})

$$\tag{2}$$

T = Absolute temperature of the radiating body ($^\circ K$)

The total power emitted by a spherical radiating body (radiance power) is:

$$R = \epsilon \sigma T^4 A_T \tag{3}$$

where A_T is the total surface area of the spherical radiating body. Thus, the total power varies with the absolute temperature, emissivity and surface area of the body. Of these variables, the absolute temperature is the most significant, since its effect is a function of its fourth power. For most efficient system design, each of these variables should be quantitatively predictable for the penetration products resulting from meteoroid impacts.

Existing knowledge of the emissivity temperature and effective radiating area of the products of penetration is fragmentary. Consequently, various estimates of these characteristics were made in the course of this study, and where applicable, these estimates were correlated with the experimentally observed results.

1. Emissivity of Penetration Products

The emissivity of the penetration products is estimated to be approximately 0.2, which is the known value of the emissivity for aluminum at 1000 C. (see Reference 7). It is assumed that the penetration products have grey body radiation characteristics (i.e., emissivity remains constant for all wavelengths). It may be noted that the emissivity for pure metals theoretically varies linearly with absolute temperature. Then the Stefan-Boltzmann equation predicts that the radiance is proportional to the fifth power of absolute temperature, in contrast to the fourth power relationship for black body radiation. An expression for the radiance of pure metals is given by Jakob (Reference 8, page 45). However, for purposes of analysis, a constant emissivity of 0.2 is assumed.

2. Area of Penetration Products

The total surface area of the products of meteoroid penetration is not precisely determinable by existing knowledge. At the instant of impact, some of the wall material will be projected outward from the front surface, in the direction opposite to the direction of meteoroid travel (see Reference 9). Additional material is ejected from the back surface of the wall. The total volume of material displaced may be determined from the hole diameter and hole shape after impact. However, the manner in which this ejected volume is divided between the front and the rear surfaces is not precisely known, nor is the degree of fragmentation of the material leaving the rear wall.

The limitations of currently available theoretical and experimental knowledge in these areas requires that estimates be made of the effective radiating surface area of the material ejected from the rear surface of the wall. For non-penetrating impacts, Eichelberger & Gehring (Reference 2) have shown that the volume of the

crater produced is proportional to the kinetic energy of the impacting particle and accordingly for a hemispherical crater, the crater diameter varies with the two-thirds power of the velocity. Eichelberger also has obtained photographs showing a distribution of penetration products that reasonably approximates a spherical shape with the diameter of the sphere equal to the diameter of the hole in the wall (Figure 11). Therefore, in subsequent analyses in this report, it is assumed that the penetration products radiate like a sphere of diameter equal to the hole and with an emissivity of 0.2.

3. Temperature of Penetration Products

The effective radiating temperature of the penetration products is one of the most important and yet one of the most elusive parameters which affect the design of an infrared detection system. Two of the important questions which have not yet been adequately investigated are:

a) What fraction of the kinetic energy of the impacting particle is converted into internal energy of the penetration products?

b) Are the penetration products at a fairly uniform temperature and all of a single phase (solid or liquid) or are parts of the ejected material in the gaseous or plasma phase?

An estimate of the average temperature of the penetration products may be obtained from consideration of the conservation of energy of the impacting particle. A fraction β, of the total kinetic energy will be transformed to thermal internal energy according to the relationship:

$$\beta \frac{1}{2} m_p V^2 = W C_p \Delta T \tag{4}$$

Fig. 11 - Residual Pellet and Spall Pattern 10 μsec After Impact On 0.32 cm Thick Aluminum (2024) Meteor Shield by a 0.18 gm Steel Pellet Striking at 5.01 km/sec.

FIGURE 11

- 25 -

where

m_p	=	Mass of the impacting particle (grams)
V	=	Velocity of the particle at time of impact (cm/sec)
W	=	Mass of the material removed by impact (assumed much larger than the mass of the impacting particle)
C_p	=	Average specific heat of the wall material over the appropriate temperature range
ΔT	=	Change in average temperature of the displaced wall material, as a result of impact ($^\circ$K)

The value of β is not known. However, Eichelberger states (Reference 10) that from 70 percent to 90 percent of the incident kinetic energy is converted to plastic strain energy in the target, in which case less than 30 percent appears as internal energy of the ejected material. In this case, if one uses Eichelberger's empirical data for the mass of material ejected as a function of particle kinetic energy (Reference 10), and assumes $\beta = 0.3$, the average temperature of penetration products is calculated to be only a few hundred degrees Centigrade. (Crater data in Reference 10 were supplied by Eichelberger to correct his data of Figure 10 in Reference 2, which we found to be inconsistent with his data in Figure 12 of Reference 2). An effective radiating temperature of a few hundred degrees Centigrade is much too low to explain the large infrared signals observed in our penetration experiments. Therefore, it is tentatively concluded that the penetration products must include some material at very high temperature. An estimate of the effective radiating temperature of the penetration products was obtained by a procedure which utilized empirical values of the voltage signal observed in penetration experiments together with manufacturers performance data for the lead sulfide sensor. Using this procedure, and assuming the penetration products behave like a sphere of diameter equal to the puncture and with an emissivity

of 0.2 it was calculated that the effective temperature of the source would have to be approximately 3000 K. to account for the observed signal voltage when firing into an air-filled tank.

Experiments have been conducted by Space Technology Laboratories (Reference 11) in which very small micron size particles impact on an aluminum film covering a photomultiplier tube and the amplitude of the PM tube signal is correlated with particle mass and velocity. In this case, the particle penetrates through aluminum into glass and the maximum irradiance received by the photocathode is that emitted by material at the bottom of a non-penetrating crater. Therefore, their data may not be directly applicable to the case of penetrations through aluminum plates. However, it is interesting to note that their PM tube signal voltage per unit mass of the incident particle increases approximately with the fourth power of the impact velocity. It is expected that detailed analysis of the STL data, taking into account the spectral response of the PM tube and the variation in diameter of the aluminum film penetration might permit an approximate determination of the effective temperature of the crater material and its variation with impact velocity. If the source temperature is known, the irradiance at a range, s, from a spherical source of radius, r, can be found from the equation:

$$H = \frac{\epsilon \sigma T_s^4}{(s/r)^2} \tag{5}$$

This equation is plotted in Figure 12 for a black body ($\epsilon = 1$). A range scale is also shown that relates range to s/r for the case of a spherical source of radius 1 mm.
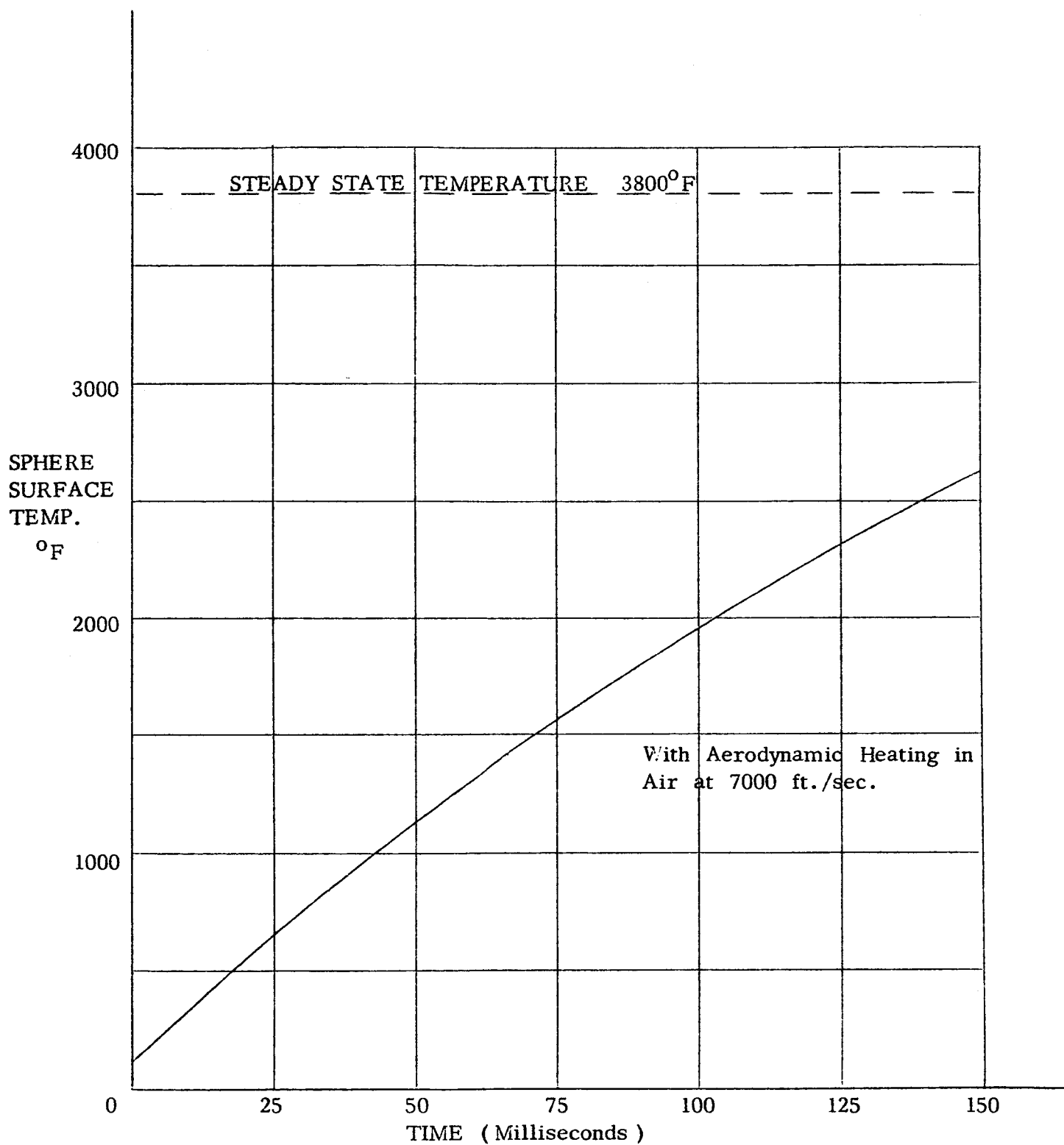
SPHERE SURFACE TEMPERATURE vs. TIME

Figure 12

4. Aerodynamic Heating of Penetration Products

An analytical study was made to determine whether aerodynamic heating of penetration products might produce significant changes in particle surface temperature which would affect the infrared radiation detected.

As an example, it is assumed that a 1/16 inch diameter sphere of aluminum from the tank wall enters a tank filled with air at a velocity of 7000 feet per second. The heat flux at the stagnation point is approximately: (Reference 12)

$$q_w \quad = \quad f_2 \sqrt{\beta \, \rho_\infty \, V_\infty} \quad C_p \, (T_0 - T_w) \tag{6}$$

where:

$$f_2 \quad = \quad 0.763 \, (Pr)^{-0.6} \cong 0.92 \text{ for air}$$

$$\beta \quad = \quad \frac{1.1 \, V_\infty}{D} \text{ at Mach numbers above 6}$$

$$T_0 \quad = \quad \text{stagnation temperature}$$

$$T_w \quad = \quad \text{wall temperature}$$

$$V_\infty \quad = \quad 7000 \text{ feet per second}$$

$$D \quad = \quad \text{sphere diameter - 1/16 inch}$$

the stagnation temperature is:

$$T_0 \quad = \quad T \left(1 + \frac{k-1}{2} M^2 \right) \quad = \quad 4570 \text{ R.} = 4110 \text{ F.} \tag{7}$$

for an air temperature of 520 R. If the sphere were isothermal at each instant and the heat flux were uniform and equal to the value at the stagnation point, its initial rate of temperature rise would be:

$$\frac{dT}{dt} \quad = \quad \frac{q_w}{\rho C} \, (3/r) \tag{8}$$

which is calculated to be 21 F. per millisecond for an initial sphere temperature of 60 F.

The steady state sphere temperature is given by equating convection to radiation heat flux:

$$q_w = h(T_o - T_w) = \epsilon \sigma T_w^4 \tag{9}$$

where:

h = heat transfer coefficient $\approx$ 970 Btu/hr-ft^2-F.

ϵ = sphere emissivity $\approx$ 0.5

σ = Stefan-Boltzmann constant

Solving for the steady state temperature by trial and error:

$$T_w = 4275 \text{ R}. = 3810 \text{ F}.$$

The time-variation of sphere surface temperature is estimated by the use of Groeber's charts as given by Jakob (page 281 of Reference 8) which permit calculation of sphere surface temperature following a step change in ambient temperature, neglecting radiation heat loss. By assuming that the dimensionless surface temperature varies with time as given by Groeber, but that the maximum steady state temperature is 3810 F. instead of the full stagnation temperature of 4110 F., the surface temperature varies with time as shown in Figure 13. It is seen that the change in sphere surface temperature during the few milliseconds that the sphere may remain in the view of an infrared sensor, will be very small. Therefore, it is concluded that the radiation from penetration products will be determined primarily by their temperature at the instant of puncture, and aerodynamic heating will have a negligible effect in changing the particle temperatures, for velocities below 7000 feet per second.

Irradiance at Sensor (H) (microwatts /cm^2)
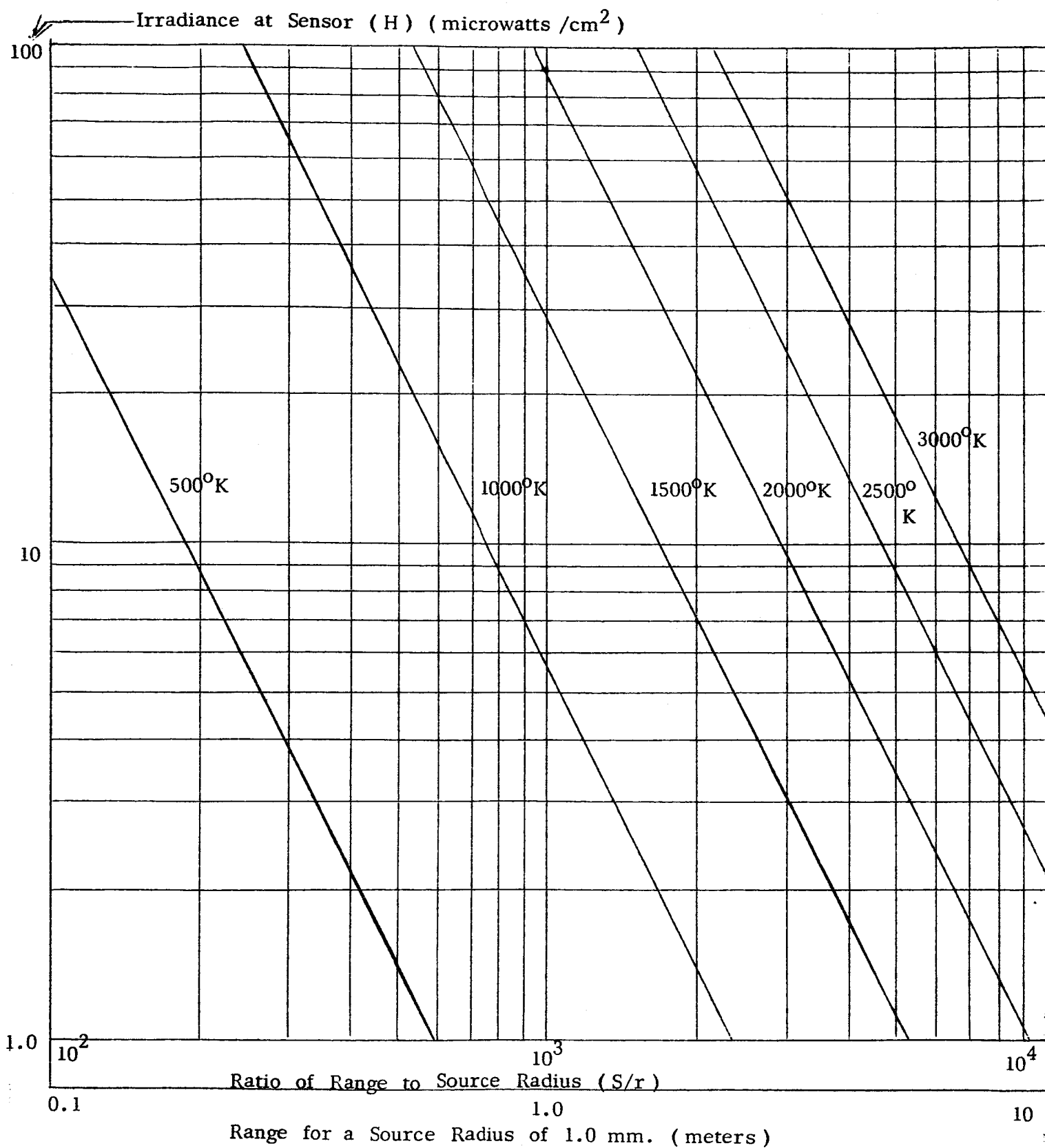
IRRADIANCE AT SENSOR PRODUCED BY A BLACK BODY SOURCE AT TEMPERATURE T$_S$ AS A FUNCTION OF RANGE

FIGURE 13

A preliminary estimate was made to determine whether thermal radiation from the gaseous boundary layer surrounding penetration products would contribute a significant infrared signal as compared to the thermal radiation emitted by the solid or liquid penetration products themselves. It was tentatively concluded that for velocities of the penetration products of less than 8000 feet per second, the gaseous boundary layer radiation is negligible even in a strongly radiating gas such as CO_2 or H_2O. However, for penetrations by real meteoroids, the velocity of penetration products might exceed 8000 feet per second and more detailed study is required to determine whether radiation from a plasma sheath will be significant and if so, how it varies for various types of propellants. For impacts into an oxygen environment, it is expected that radiation produced by chemical oxidation will substantially exceed that produced by plasma sheath radiation alone, in the absence of chemical reactions.

B. Optics

In a majority of optical system designs, the objective is to focus radiation from sources lying on or adjacent to the axis of the optical system. Such designs include the normal telescope, infrared homing, and solar energy collecting applications. Accordingly, many optical collecting systems utilize paraboloidal or spherical mirrors. The most desirable characteristic of the paraboloid is its ability to concentrate to the focal point all incident radiation parallel to the mirror axis, regardless of the displacement from the axis of any particular incident photons. The spherical mirror is an efficient collector only for radiation that is both parallel to, and close to, the mirror axis.

Each of these mirror types, however, is limited in efficiency for collecting radiation from off-axis sources. In the case of the paraboloid of revolution,

radiation from off-axis sources, rather than being concentrated to the focal point, is spread over an area, the size of which varies with the angular displacement of the source from the mirror axis. It is apparent that the required sensor size will become large in order to detect targets that are significantly displaced from the mirror axis. In the case of the paraboloidal as well as the spherical mirror, radiation from off-axis sources may undergo multiple reflections on the mirror surface and be reflected out of the mirror without striking the sensor.

In the design of a meteoroid detection system for a propellant tank, it should be recognized that the highest temperature sources resulting from a meteoroid impact will be located at or adjacent to the tank wall. It is expected that penetrating materials will cool as they move away from the impact area into the tank volume. The cooling rate of such materials will, of course, be greater when a cryogenic liquid is inside the tank. It is therefore desirable that the optical design of the penetration detection system provide good collecting efficiency for off-axis radiation, in order to minimize the number of sensors needed to provide surveillance of the entire inner surface of a tank wall.

Consideration is given to cylindrical tank geometries in which it is desired to monitor the entire inner surface with a minimum of internally mounted sensors. Practical considerations of installation and space utilization indicate that a preferred system design should provide two sensors, one at each end of the tank near the axis and optically designed to monitor the opposite half of the tank surface. Under such conditions each sensor may be mounted with the plane of its sensitive area perpendicular to the axis of the cylinder. Figure 14 illustrates such a sensor mounting.
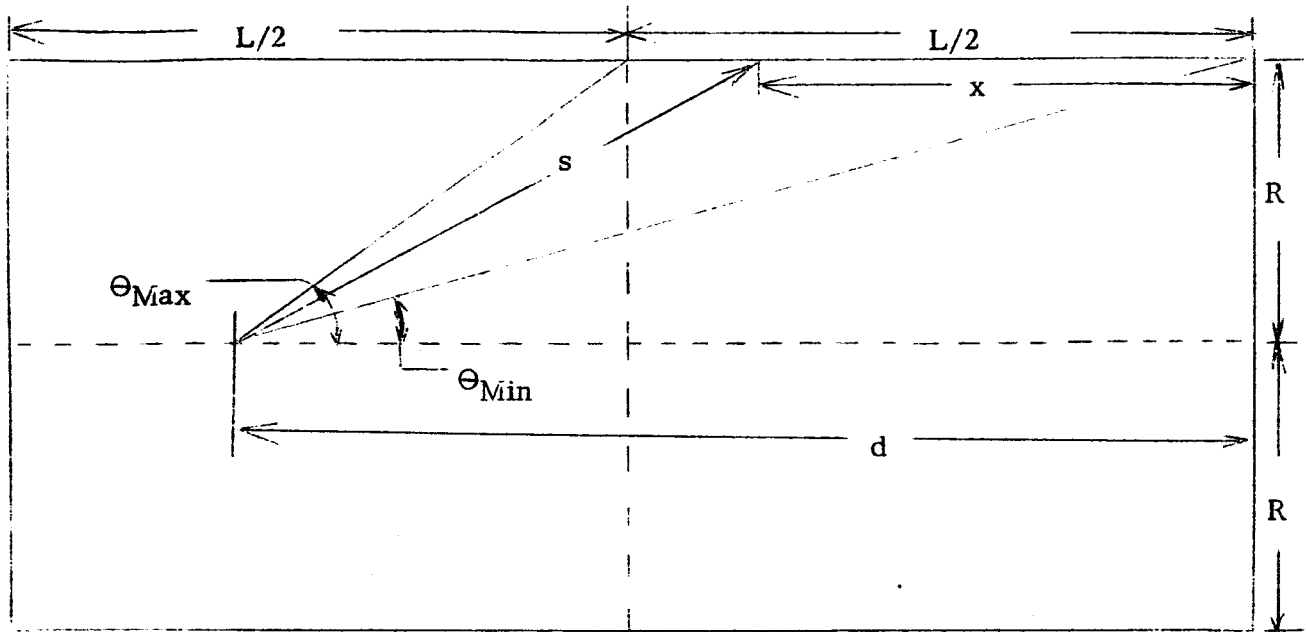
SENSOR MOUNTING GEOMETRY

FIGURE 14

The parameters in Figure 14 are:

R	=	radius of tank cross-section
s	=	distance (range) from sensor to point of meteoroid impact
θ	=	angle between cylinder axis and line joining sensor to point of meteoroid impact
L	=	length of tank
x	=	distance to point of impact from wall opposite sensor

Radiation incident upon the sensor from the point of impact will vary inversely with the square of the range and directly with the cosine of the angle of incidence:

$$H = \frac{E_o}{s^2} \cos \theta \tag{10}$$

where

H =   irradiance, radiant power per unit area of the sensor surface

E_o =   radiant intensity of the source per unit solid angle

It may now be assumed that E_o is constant for any value of x, that is, the analysis is directed toward sensor optical characteristics required for impacts of equal magnitude occurring anywhere along the tank wall. The distance, s, from the source to the sensor may be expressed as a function of the constant radius, R, and θ:

$$s \quad = \quad \frac{R}{\sin \theta} \tag{11}$$

substituting in Equation (10):

$$\frac{H \, R^2}{E_o} \quad = \quad \sin^2 \theta \, \cos \theta \tag{12}$$

Since R^2/E_o is a constant, H varies with θ only. Then the maximum value of H as a function of θ may be found by equating the first derivative of the function to zero, which gives the result that H is maximum when

$$\tan^2 \theta \quad = \quad 2$$

or,

$$\theta \quad = \quad \tan^{-1} \sqrt{2} \quad = 55^o \tag{13}$$

This indicates that the maximum irradiance at the sensor from a source located on a cylinder occurs at a view angle of $\theta = 55^o$. Figure 15 is a plot of the irradiance function, $X = \frac{HR^2}{E_o} = \sin^2 \theta \cos \theta$, as a function of θ.

It may be seen that the sensor may be positioned so that X is of equal magnitude at each extremity of the required field of view of the sensor. For example,
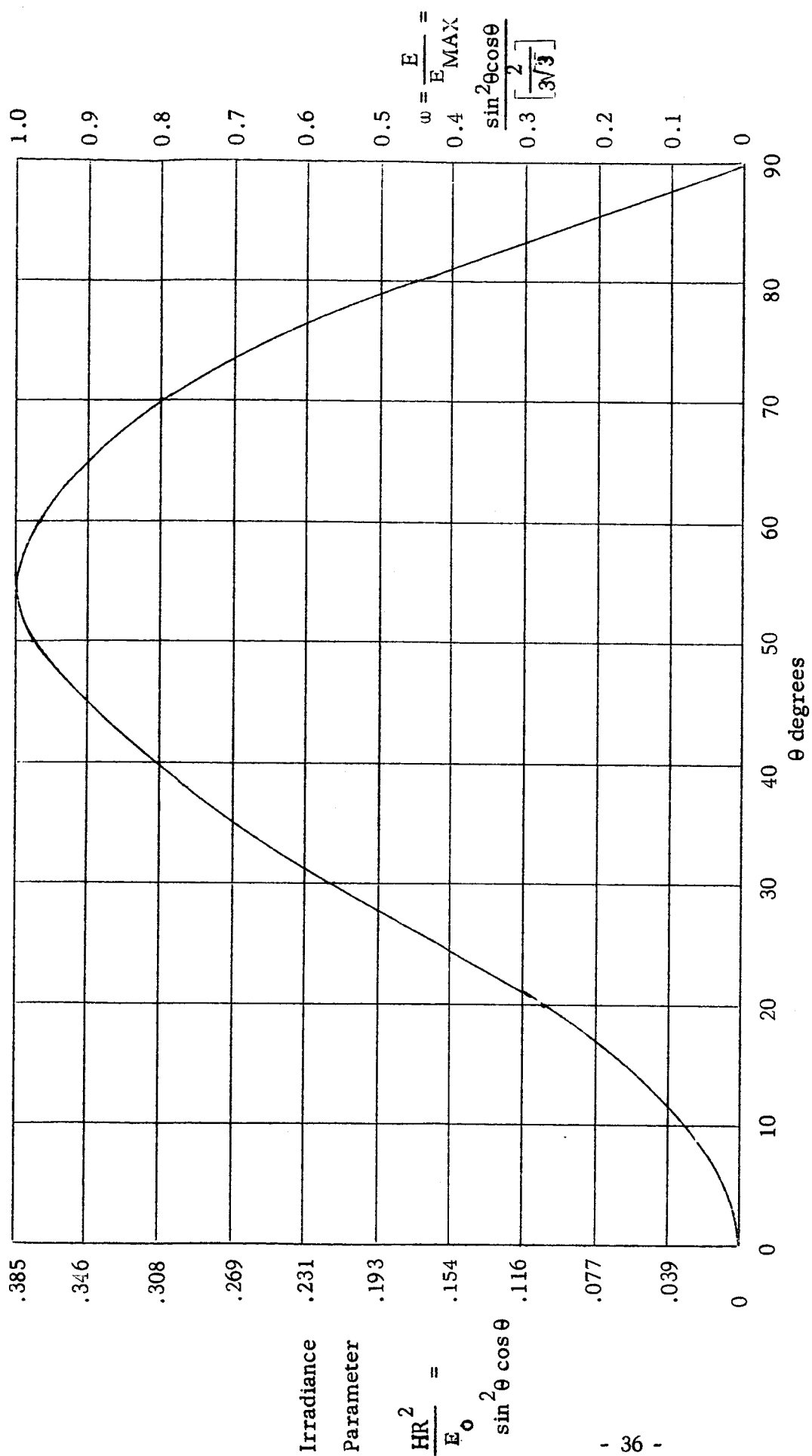
IRRADIANCE PARAMETER AS A FUNCTION OF INCIDENCE ANGLE

FIGURE 15

$\omega = \dfrac{E}{E_{MAX}} = \dfrac{\sin^2\theta\cos\theta}{\left[\dfrac{2}{3\sqrt{3}}\right]}$

θ degrees

Irradiance Parameter

$\dfrac{HR^2}{E_o} = \sin^2\theta \cos\theta$

assume that the sensor is to monitor a length $L/2$ of tank wall, and further that this wall length may be subtended by a view angle defined between $\theta = 44^\circ$ and $0 = 64^\circ$. Then the irradiance at the sensor will be equal for radiation incident from each end of the region under surveillance while radiation from other points will produce slightly higher irradiance. Under these conditions the sensor optics are optimized, since values of irradiance are obtained which are as large and as uniform throughout the field of view as is theoretically attainable.

For propellant tanks with hemispherical or domed ends, it is expected that in most cases the domed ends will be protected from meteoroid puncture by a cylindrical fairing which comprises the vehicle skin. Therefore, puncture of the ends would be much less probable than puncture of the cylindrical surface. If punctures in the ends are to be detected it can be seen that the detection sensitivity for the domed head region will be approximately equal to that obtained at the end of a truly cylindrical tank of equal volume.

To determine the optimum axial position of the sensor in a cylindrical tank the following procedure may be used. Select a fraction, ω, of the maximum irradiance that will be acceptable at one end of the required length to be monitored, $L/2$. Then enter the curve in Figure 15 from the right to determine the maximum angle of incidence θ_{MAX}. Thus, for ω chosen as 0.8, θ_{MAX} is read from the curve as 70°. Next, extract the minimum incidence angle, θ_{MIN}, permissible at the chosen ω, by reading on the same horizontal line the point on the curve to the left of the θ_{MAX} point. For $\omega = 0.8$, the value of θ_{MIN} is 40°. Then, it is necessary to assure that the angle subtended between θ_{MIN} and θ_{MAX} is sufficient to include the entire length $L/2$, for any particular tank geometry. The minimum angle that θ_{MIN} can assume to view the extreme end of the cylindrical wall is seen to be:

$$\theta_{MIN} = \tan^{-1} R/d \tag{14}$$

where:

R = tank radius

d = axial distance from end of tank to sensor location.

Thus, for the example given, the sensor should be located at:

$$d = \frac{R}{\tan 40^\circ} .$$

(15)

It is recognized that no optical gain is attainable in a sensing system that does not provide refractive or reflective collecting elements. However, there are several reasons why this is not injurious to the overall system design. These reasons are discussed below:

1. Practical limitations on the size of collecting elements restrict the amount of optical gain that ideally may be attained. It would be impractical to use large mirrors or lenses inside propellant tanks, as they would require correspondingly large support structures, and pose installation problems. High optical gain requires a large collector and a small sensor. However, with a paraboloidal or spherical collector, a small sensor is not feasible for detecting off-axis sources and the sensor area must be increased substantially to intercept off-axis radiation. Therefore, the sensor size tends to approach the collector size and the optical gain achieved is small, thereby making it preferable to use a plane sensor without a collector for simplicity. In addition, by increasing the sensor area, the signal-to-noise ratio of the sensor is improved. (Reference 6) Therefore, the area of the sensitive surface of the sensor may be increased to provide as much collecting surface as would be attainable with small collecting mirrors or lenses.

Such a design using a fairly large sensor surface will result in improved system performance, both optically, by the elimination of reflection or absorption losses from optical elements, and electrically, by the improvement in the signal-to-noise ratio of the sensor.

2. The state of the art regarding infrared systems design is such that signal amplification by many orders of magnitude may be readily achieved electronically. Since the total optical gain attainable is only of the order of 10 to 1000, compensation for any losses in optical gain may be made quite easily by increases in the voltage gain of the amplifier. This conclusion assumes that the noise introduced by the amplifier can always be kept below that of the sensor by proper design of the first amplifier stage.

Investigation of Radiation Transmission Through Propellant Fluids

An investigation was conducted to determine the transmission characteristics of propellant fluids for various wavelengths of electromagnetic radiation. The investigation included a literature search and personal consultation with members of the staff of Infrared Industries, Incorporated, the University of Michigan, and The Applied Physics Laboratory of John Hopkins University. The objective was the determination of absorption coefficients per unit path length for liquid and gaseous oxygen, hydrogen, nitrogen tetroxide, and hydrazine for various wavelengths of radiation.

The investigation did not reveal any prior systematic studies directed toward the same objectives. However, several references were found in which the absorption characteristics of each of the propellants were treated separately. Generally, it may be concluded that no serious absorption problems are to be expected for hydrogen or oxygen within the frequency band to be utilized in the detector system (visible through 3μ). Pertinent graphs and extracts from the references are indicated below.

- 39 -

1. Hydrogen (Reference 13)

The graph in Figure 16 shows absorption due to intermolecular forces of gaseous and liquid hydrogen occurring in the region from 1.9μ to 2.4μ. Hydrogen, however, is essentially transparent through the visible and out to approximately 1.9μ. Although an absorption band is expected in the regions shown in the graph, this region should represent only a small portion of the frequency band of interest in a detector system.

From Figure 16 it may be estimated that radiation between 1.9 and 2.4 microns will undergo absorption in liquid hydrogen at 18 K. with an absorption coefficient of approximately 0.8 cm^{-1}, which corresponds to an intensity reduction by a factor of 10 in a thickness of 2.8 cm. For a black body source at 1000 K., the fraction of the emitted radiation between 1.9 and 2.4 microns is only about 10 percent of the total, or about 1/3 of the radiation below 3μ, which is within the response region for a typical PbS detector. Therefore, this absorption should not be a severe obstacle to the detection of a source at 1000 K. through a long path of liquid H_2.

2. Oxygen (Reference 14)

The graph in Figure 17 shows intermolecular absorption of oxygen at wavelengths of 5.7μ to 7.5μ, which are much longer wavelengths than those of interest. Except for two discrete absorption lines at 0.78μ 1.24μ, oxygen is essentially transparent from the visible and out to approximately 5.7μ, and therefore no significant absorption from oxygen need be considered for detectors which respond to wavelengths below 5.7μ.

3. Dinitrogen Tetroxide (Reference 15)

The absorption spectrum of liquid dinitrogen tetroxide (N_2O_4) has been investigated by Snyder & Hisatsune (Reference 15) over the range of wavelengths from 2.5μ to 17μ (see Figure 18). There are several strong infrared absorption
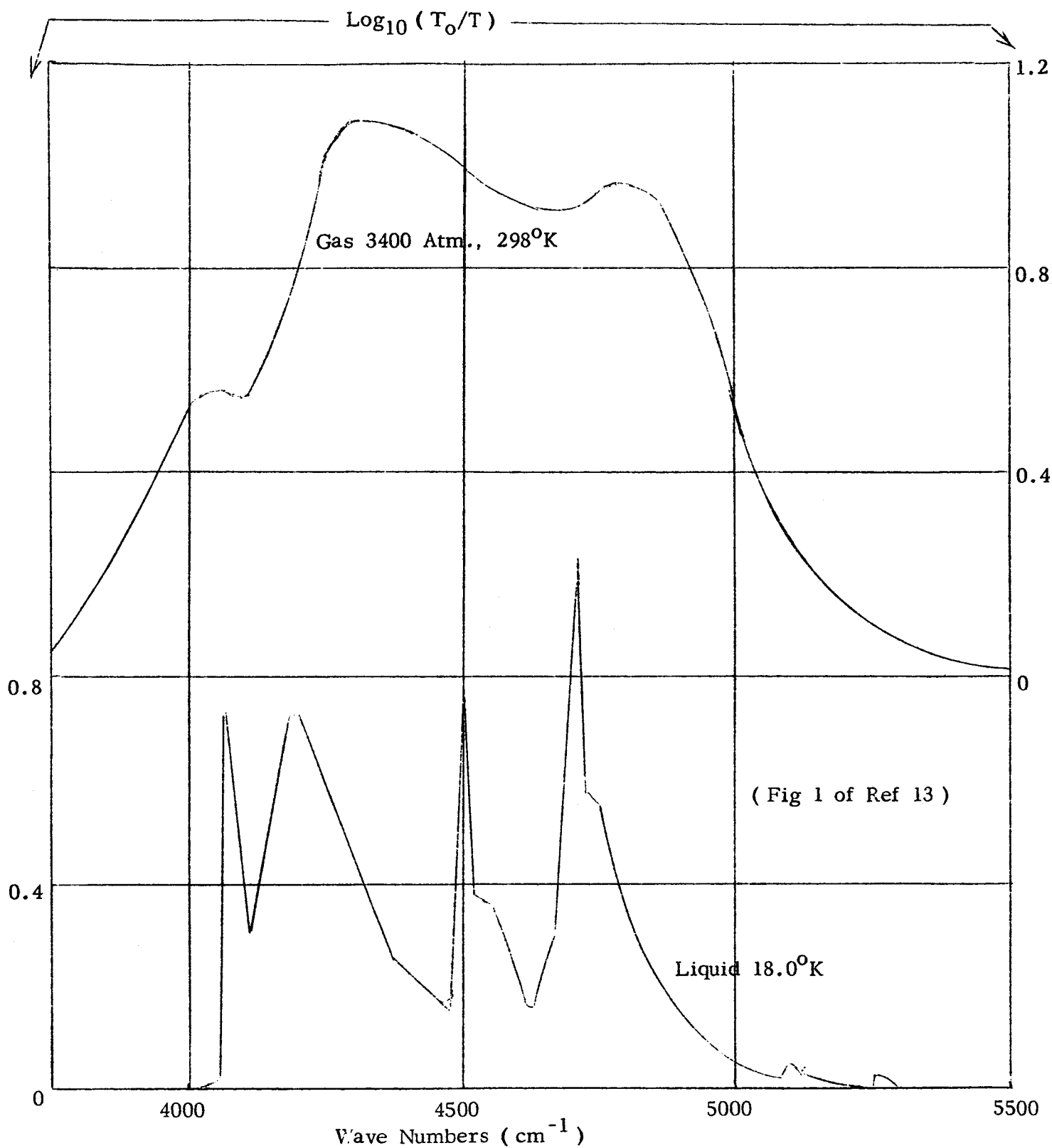
INFRARED ABSORPTION OF HYDROGEN INDUCED BY INTERMOLECULAR FORCES

FIGURE 16

(Figure 2 of
Ref. 14)
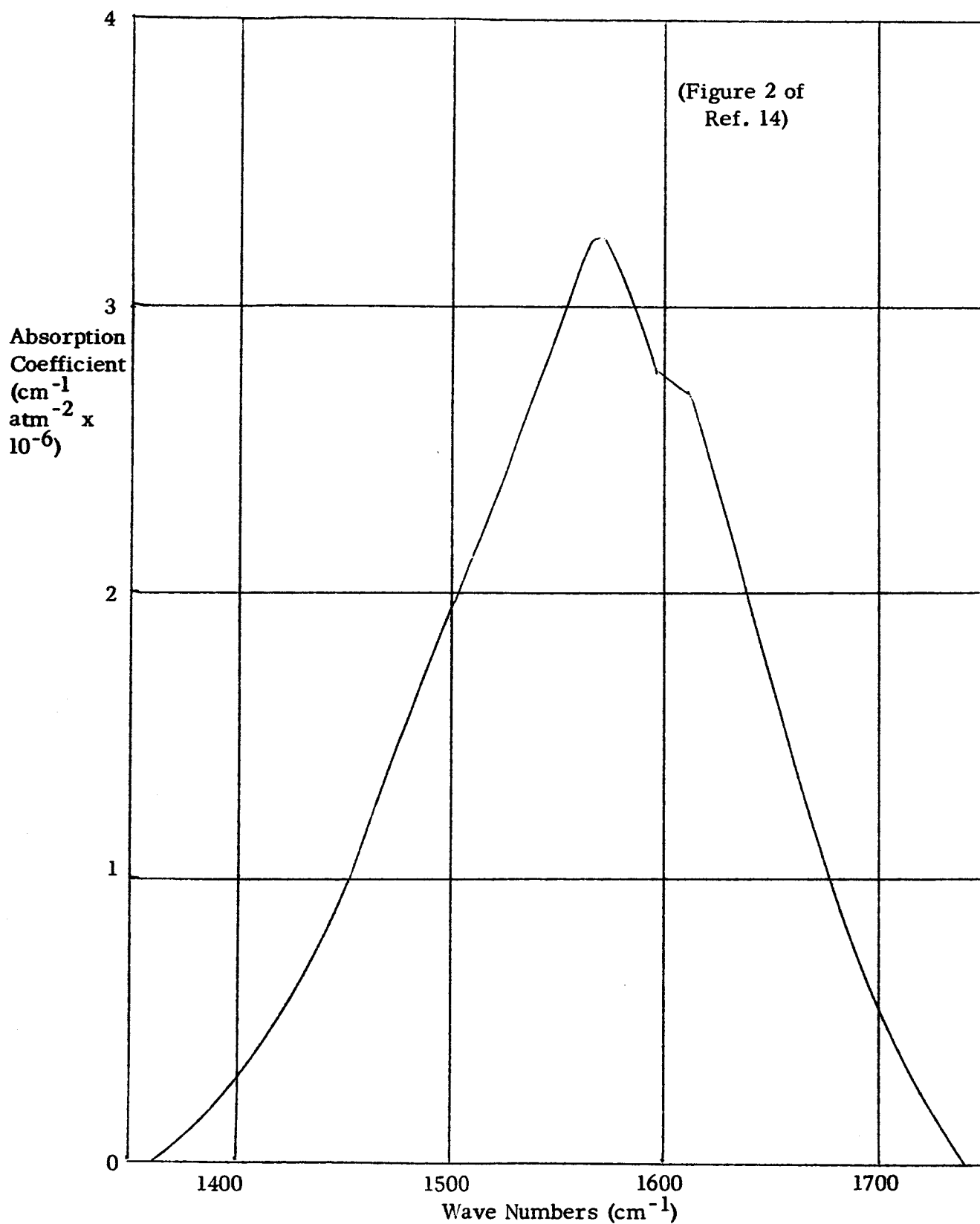
ABSORPTION OF GASEOUS OXYGEN
FIGURE 17

(Figure 3 of Ref. 15)

Trans-mission (%)

Wave Number (cm^{-1})
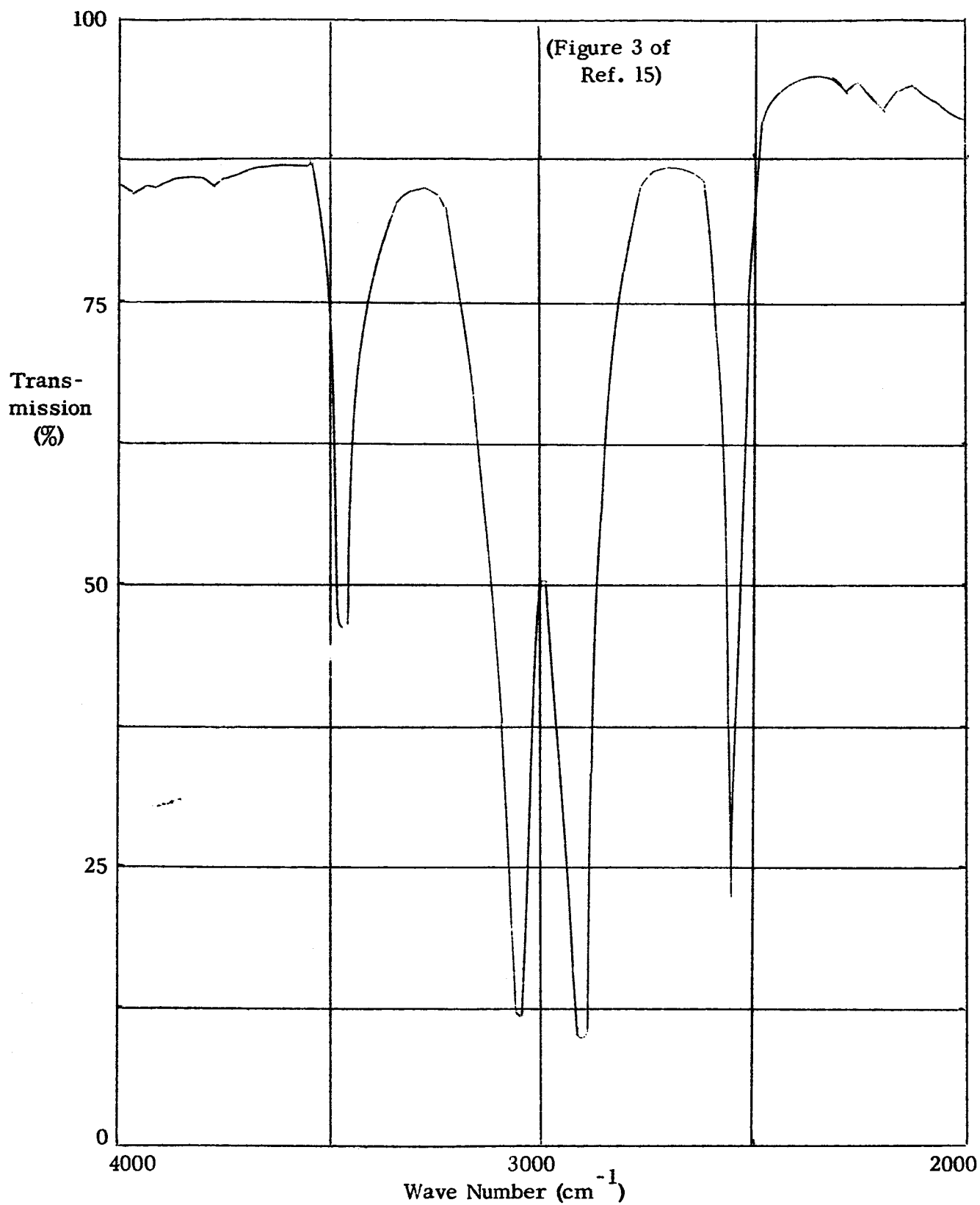
SPECTRUM OF LIQUID N_2O_4 IN 0.1 MM CELL   FIGURE 18

ABSORPTION SPECTRUM OF HYDRAZINE IN CONDENSED PHASES

FIGURE 19

lines and bands which indicate very poor transmission of these wavelengths through path lengths as short as a few millimeters. No data were found on the transmission of visible light or near infrared radiation through liquid $N_2 O_4$. However, since the components nitrogen and oxygen are essentially transparent, no significant absorption is expected for $N_2 O_4$ at wavelengths below 2.5μ.
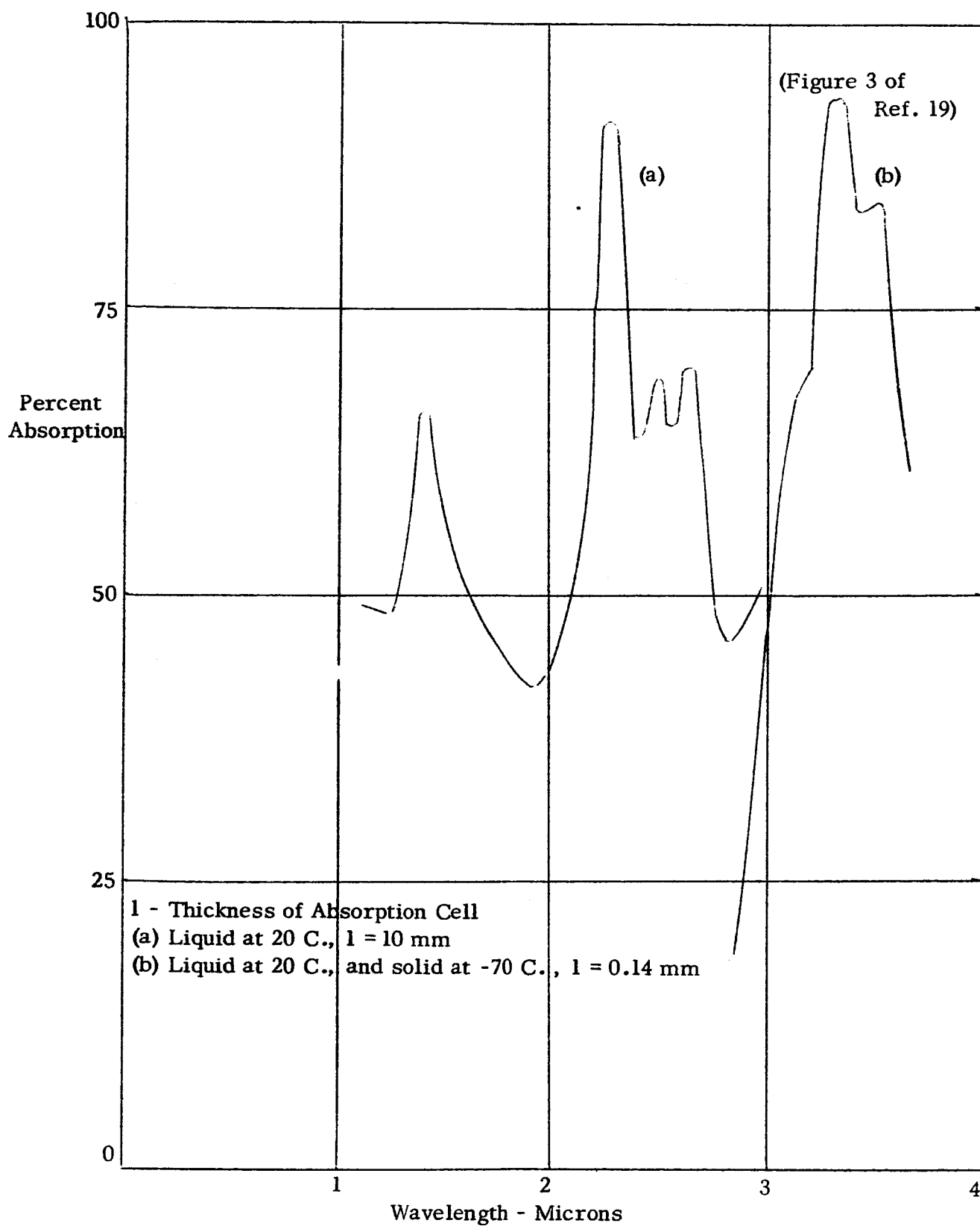
4. Hydrazine (Reference 16)

Data by Giguère and Liu (Reference 16), as shown in Figure 19, indicate strong absorption by liquid $N_2 H_4$ at several wavelengths between 1μ and 3μ and also between 6μ and 14μ. However, transmission of visible and near infrared radiation out to 1μ is expected to be quite good.

No absorption data were found for unsymmetrical dimethyl hydrazine (UDMH) which is often used as a fifty percent additive to hydrazine for storeable propellant applications. However, theory would predict many infrared absorption lines. Further investigation is required to determine the feasibility of detecting visible and near infrared radiation through long path lengths in typical mixtures of UDMH and $N_2 H_4$, such as Dymazine or Aerozine.

C. Sensor Characteristics

A review of the performance characteristics of available sensors for the detection of infrared and visible radiation indicated that lead sulfide photoconductive sensors and silicon photovoltaic sensors were most likely to have the desired characteristics and to be commercially available at reasonable cost. Therefore, experiments were conducted with these two types of sensors.

The experimental results indicate that lead sulfide photoconductive sensors are well suited to detection of penetrating impacts with impact velocities near 7500 feet per second as obtained in this experimental program. Lead sulfide sensors were experimentally shown to be more suitable than were the silicon photovoltaic cells because of their larger voltage output and their ability to detect penetrations through an internally insulated tank wall, similar to that of the S-IV stage. The primary factors affecting the selection of a suitable sensor are discussed below. Performance, cost, reliability and general system compatibility factors, as they relate to the requirements of a meteoroid penetration detection system, are discussed for alternative sensor materials. A calculation is shown for determination of the detection sensitivity and signal-to-noise ratio, based upon assumed conditions for the radiant source, and performance data for lead sulfide sensors.

1. Sensor Performance

It has been shown previously that the penetration products for certain impact velocities may attain a temperature of 3000 K . For a black body source , the peak intensity of radiation occurs at a wavelength determinable by Wien's Law:

$$\lambda_{MAX} = \frac{2893\,\mu - {}^{\circ}K}{T\,({}^{\circ}K)} \tag{16}$$

At 3000 K. the value of λ_{MAX} is 0.965 micron. Higher temperatures will produce peak radiation intensities at shorter wavelengths, and lower temperatures will produce peak intensities at longer wavelengths. Therefore the sensors used for meteoroid penetration detection should be responsive to radiation of wavelengths in the near and intermediate infrared. Lead sulfide sensors can be manufactured so that their frequency response characteristics are essentially flat for radiation ranging from the visible band through the infrared to about 3 microns wavelength, and therefore they are well suited to this application.

Signal detection in photoconductive sensors is based upon detection of increase in conductivity of the sensor caused by incident radiation. In order to detect incident radiation, a constant electric potential is maintained across the sensor, so that decrease in resistance of the sensor will induce a corresponding increase in current flow through it. The increase in sensor conductivity results from the creation of free electron and free hole carriers by absorption of incident photons within the material of the sensor. The characteristics of commercially available sensors have been described elsewhere in detail (see References 6, 17, and 18). The sensor Figures of Merit that are worthy of note are the detectivity, responsivity, time constant, and resistance.

Detectivity (D*) is defined as the ratio of the square root of sensor area divided by the Noise-Equivalent-Power of the sensor. The Noise-Equivalent-Power (NEP) is the incident radiant power required to create a signal-to-noise ratio of unity as measured under standard conditions of modulation frequency, bandwidth and source temperature. The detectivity is thus a measure of "sensitivity" in detecting small values of radiation flux. The detectivities of lead sulfide sensors compare very favorably with those of alternative materials such as I_N Sb and PbSe (Reference 6) for wavelength range of interest. Current noise is the primary source of noise in PbS sensors.

- 47 -

The responsivity of a sensor is defined as the RMS signal voltage per unit RMS radient power incident upon the sensor and is expressed in volts per watt. It is a function of the source temperature, sensor temperature, and sensor resistance for a given type of sensor.

The time constant of the sensor is the time required for the signal to build up to $(1 - \frac{1}{e})$ times its maximum, or decay to $\frac{1}{e}$ times its maximum, upon exposure to, or removal from, a standard radiant flux. It should be noted that the time con-- stants for lead sulfide may vary over a range from 10 to 1000 microseconds at toom temperature, and from 100 to several thousand microseconds at cryogenic temperatures. Short time constants are desired for meteoroid impact detection to permit the most rapid sensor response to the penetration products when they exist at their highest temperatures adjacent to the tank wall and to make possible the identification of a penetration by the rapid **rise** in infrared signal at the first instant of penetration. However, since the detectivity is proportional to the square root of the response time, the detector should have the longest time con- stant consistent with the frequency response requirements to obtain the highest possible detectivity. For operation at liquid oxygen temperatures, lead sulfide sensors may be manufactured with time constants of 100 microseconds, with some- what larger values when operated at liquid hydrogen temperatures.

The resistance of the sensor determines the optimum input impedance of the system amplifier. Practical amplifier design requires that the input impedance lie some- where within the range from several hundred ohms to 1 megohm, as very low input impedances may require transformer coupling for proper matching, and higher input impedances have associated problems of electrical pickup and microphonic noise. The resistance of the sensor may be controlled to predetermined values through material selection and electrode placement in the manufacturing process. Flexibility of design is thereby permitted in the input impedance of the system amp- lifier.

A comparative study of performance of alternative sensor materials that are responsive to the near infrared has been reported by Anderson (Reference 19). Significantly, the report states that for operation at liquid nitrogen temperature, lead sulfide is a better detector of sources at temperatures of 300 K. or higher, than the other detectors investigated, in terms of noise equivalent power. The other materials studied were lead selenide, germanium, and indium antimonide, all of which have some response to longer wavelengths than the cut-off wavelenth for lead sulfide. Improvements in performance of doped germanium and indium antimonide sensors have been reported in the last few years. However, any resulting performance advantages in these materials, as compared with lead sulfide, are negated by the cost and system compatibility factors discussed below.

Thermistor bolometers are actuated by temperature rise, rather than excess carrier formation, and have appreciably slower time constants than the photo-conductive sensors. The bolometers are also appreciably more costly, as is indicated below.

2. Sensor Costs

The following cost tabulation is based upon the best estimates obtainable, for sensors in procurement lots of 50 to 100. The information has been provided by Infrared Industries Incorporated (Mr. N. C. Anderson, Vice President), Texas Instruments, Inc. (Mr. Donald N. Speed, Product Marketing Manager, Materials and Sensors Department) and Barnes Engineering Company, (General Bulletin 1-100).

Sensor Material	Sensor Price Range			Sensor Manufacturer
In Sb	$400	to	$800	Texas Instruments, Inc.
Ge (Doped)	$2000	to	$3500	Texas Instruments, Inc.
PbS	$20	to	$50	Infrared Industries, Inc.
Thermistor Bolometer	$250	to	$500	Barnes Engineering Co.

3. Sensor Reliability

A principal cause of malfunction of infrared detection systems is spurious radiation in the background against which a target must be viewed. This has been observed in the performance of various homing and satellite observation devices (Reference 20). The environment provided inside a space vehicle propellant tank is ideal for infrared detection system operation, in that the inside of the tank will be dark, admitting no spurious radiation (for at least a portion of the desired useful life of the detector system prior to any punctures). In addition, the tank will be at normal room temperatures, or considerably below, if cryogenic propellants are used. If the sensor is operated at reduced temperature, the noise equivalent power may be substantially decreased, making the system more sensitive to small penetrations.

The experimental study verified that the lead sulfide sensors may be operated satisfactorily in a cryogenic fluid. In many cases they have been operated at liquid nitrogen temperature, sometimes immersed in the liquid. Lead sulfide sensors have been in quantity production for several years, so that the manufacturing processes are subject to a high degree of control. The indium antimonide and doped germanium sensors are produced in small lots, with attendant problems of quality control.

4. General System Compatibility

The lead sulfide sensors may be produced in various configurations including the flat plate type which is recommended for the meteoroid detection system. No special glass mounting tube is required, as is the case with sensors of some other materials. Therefore, there should be no difficulty in designing a sensor and light weight mounting which will withstand vibration and acceleration loads. The sensor mounting structure may be a flanged, aluminum fitting which can be attached through the wall of a propellant tank. For use with cryogenic propellants, it may be necessary to incorporate thermal insulation in the fitting to reduce heat transfer into the tank.

5. Computation of Sensor Signal-To-Noise Ratio

An example is included to derive the signal-to-noise ratio attainable when detecting a radiation pulse produced by a small 0.020 inch diameter spherical source with an emissivity of 0.2 and a temperature of 3000 K. at a range of 10 meters, neglecting radiation absorption.

The total irradiance at the sensor is calculated from the Stefan-Boltzmann Law to be:

$$H = \frac{\epsilon \, \sigma \, T^4}{(s/r)^2} = \frac{0.2 \, (5.67) \, (10)^{-12} \, (3000)^4}{\left[\frac{1000}{0.01(2.54)} \right]^2} = 0.059 \, \mu \, w/cm^2 \tag{17}$$

Assuming a one square centimeter area for the sensor with no correction for the angle of incidence, the total incident power is $0.059 \, \mu$ watt. For a lead sulfide sensor which has a flat response out to 3 microns when operated at room temperature, the noise equivalent power and responsivity may be calculated from manufacturers empirically derived standard data (Reference 17). Corrections are made to the data based on an amplifier bandwidth of 0 to 2000 cps to limit the current noise generated in the sensor, an operating voltage of 50 volts, and a sensor resistivity of 50,000 ohms. The noise equivalent power is calculated to be 8×10^{-10} watt and the responsivity 500 volts per watt of incident radiation. The output signal is then 30 microvolts and the signal-to-noise ratio is:

$$\frac{S}{N} = \frac{0.059 \times 10^{-6} \, w}{8 \times 10^{-10} \, w} = 74 \tag{18}$$

which is approximately 19 DB.

A discussion of the amplifier design requirements is given in the following section. It is shown that an input signal voltage as small as 30 microvolts is acceptable and can be detected with an amplifier voltage gain of approximately 10,000. If an increase in sensor output voltage is required, the sensor area may be increased to be greater than one square centimeter in order to provide a greater radiation collection area.

D.   Electronics

To minimize weight,power requirements and installation problems, the amplifier for the detector system should be of transistorized, printed circuit board construction.

The input circuit to the amplifier includes a series load resistor, which should be of a resistance value, R_L, equal to the dark resistance of the sensor,R, for maximum responsivity (i.e., maximum signal voltage per unit radiant flux) (Reference 5).

Figure 20 shows such an input circuit, in which a capacitor, C, serves to block DC from the base of the transistor in the first amplifier stage. For such a design the radiation incident upon the sensor would have to be optically modulated or "chopped", to provide AC input to the transistor. This chopping is in many applications provided by a rotating reticle in front of the sensor. In the meteoroid penetration detection application, transient radiation pulses are caused by individual penetrations. In some applications it may be desired to record the DC signal developed in the sensor, as this would provide a measure of the background radiation

level, which would be affected by solar radiation entering through holes from earlier penetrations, or by heat or light sources within the tank. In such cases the capacitor, C, may be removed from the amplifier input.

The voltage V_{R_L} appearing across R_L, in the absence of radiation on R, is:

$$V_{R_L} = i R_L = V_o \left[\frac{R_L}{R + R_L} \right]$$

(19)
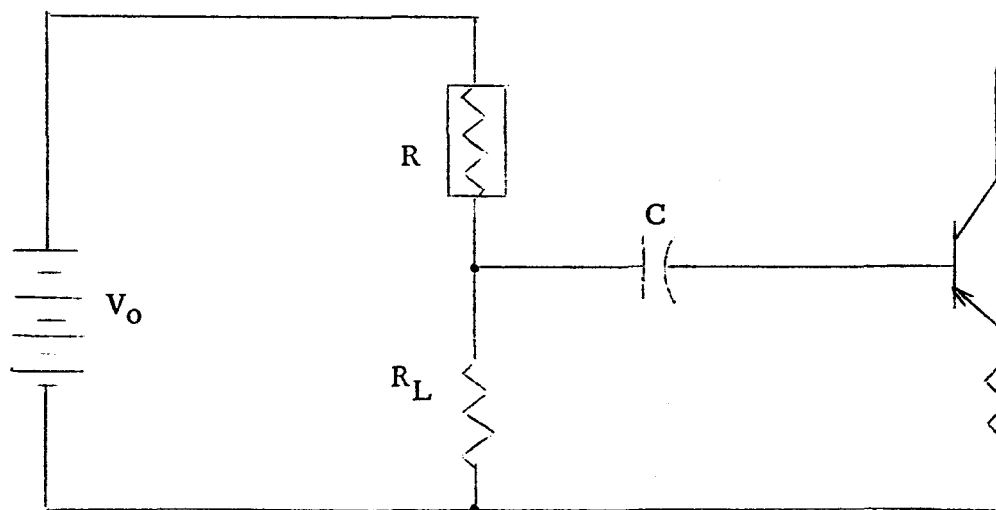
AMPLIFIER INPUT CIRCUIT

FIGURE 20

When radiation is received on the sensor, its resistance, R, is changed by an amount ΔR (which is negative). This causes an increase in current flow through the circuit and a corresponding increase in the voltage drop across the load resistor. The new voltage drop across the load resistor is:

$$V_{R_L}' = V_o \left[\frac{R_L}{R + \Delta R + R_L} \right]$$

(20)

For small changes in resistance, $\dfrac{\Delta R}{R + R_L} \ll 1$, the change in voltage across R_L is approximately:

$$\Delta V_L \cong - V_o \left[\frac{R_L \, \Delta R}{(R + R_L)^2} \right] \tag{21}$$

and for $R_L = R$:

$$\Delta V_L \cong - \frac{V_o}{4} \left(\frac{\Delta R}{R_L} \right) \tag{22}$$

Amplifier Characteristics

As indicated previously, the minimum input voltage to the amplifier may be as low as 30 microvolts for small penetrations occurring at large ranges from the sensor. Also, the maximum input voltage may be as high as several volts for large penetrations occurring close to the sensor. Therefore, it is desirable that the amplifier exhibit logarithmic gain characteristics to provide a manage-able range of output voltages.

The current state of the art permits amplifier design that provides linear voltage gain of 10,000 for voltage inputs below 10^{-4} volts, with compression of gain occur-ring for input signals greater than 10^{-4} volts. Such a design may be completely transistorized and powered by a DC battery, and produce output voltages from 0.1 to 5.0 volts.

For the case of the minimum input of 30 microvolts to the amplifier, the output voltage would be 10^4 times 30×10^{-6} volts, or 0.3 volts. This magnitude of voltage is sufficient to be detected by galvanometric or cathode ray deflection techniques, and also is sufficient to actuate solid state switching or storage circuits.

For best compatibility with a readout circuit, the output pulse should have an amplitude of at least 0.05 volt. and a rise time no longer than one-tenth milli-second. These requirements are subject to modification to meet the input requirements of a particular readout circuit.

V   CONCLUSIONS

This section summarizes the conclusions reached in the conduct of both the experimental and analytical phases of this study.

A.   Experimental

1. Both lead sulfide photoconductive infrared sensors and silicon photo-voltaic sensors can be used to detect penetrations through aluminum plates into air produced by 0.015 inch to 0.062 inch diameter stain-less steel ball bearings fired at 7000 to 8000 feet per second through vacuum at a pressure of 1 mm of Hg absolute.

2. As compared to experiments in air, the amplitude of signals from the infrared and photovoltaic sensors is increased substantially when pe-netrations are made into gaseous oxygen and decreased somewhat when penetrating into helium, indicating that a significant fraction of the emitted radiation results from the chemical reaction of pene-tration products with oxygen. The effect of oxygen partial pressure is greater on output of the silicon solar cell (which responds in a wavelength range from 0.4 to 1.1 microns) than for the lead sulfide detector (which has a relatively flat response in the visible and cut to $\sim$ 2.8 microns). Therefore, it is concluded that the light attri-butable to oxidation reactions is generally shifted to shorter wave-lengths than the radiation from the penetration products themselves in chemically inert helium. (T-304, T-305, T-306)

3. With the optical viewing geometry used in these experiments, the infrared and visible sensor response produced by light from powder

combustion products in the vacuum tank, coming through a 1/8 inch diameter hole which was open during the entire firing sequence, was too small to be detectable. Therefore, this effect is believed to produce a negligible contribution to the infrared and visible detector signal observed from an actual penetration, in which case the hole does not appear until at least one millisecond after firing the rifle. (T-451, T-452)

4. No visible radiation was observed and none could be theoretically expected from the leakage of ambient air through a 1/16 inch hole into a vacuum system at a pressure of approximately 50 mm of Hg absolute.

5. When a 1/16 inch diameter ball at 8000 feet per second penetrated a simulated S-IV tank wall, consisting of 1/8 inch of aluminum backed up by 3/4 inch of reinforced foam insulation, the penetration products were readily detected by a lead sulfide infrared sensor but gave negligible signal from a silicon photovoltaic sensor. Inspection of the large internal cavity produced inside the insulation indicated that the penetration products had expanded and presumably mixed with gas from the foam and cooled before breaking through the back of the insulation where they would be viewed by the two sensors. This result indicates that an infrared sensor is more desirable than a silicon photovoltaic sensor for detecting penetrations into an internally insulated propellant tank. (T-303)

6. The diameter of the penetration hole formed when the diaphragm was in contact with liquid nitrogen was noticeably smaller than when the diaphragm was in contact with gases at room temperature, for similar impact conditions. This result indicates that impacts into cooled walls may produce smaller penetration holes than the same impacts into uncooled walls. This observation is based upon only one data point, however. (T-307)

7. No detectible signals were observed from either sensor for impacts that did not cause penetration (i.e. perforation) of the diaphragm. This indicates that an electromagnetic radiation sensor inside a tank will not be actuated by impacts that do not penetrate the tank wall. This ability to distinguish between penetrating and non-penetrating impacts is a primary requirement for a useful penetration detection system.

B. Analytical

The most significant results and conclusions from the analytical study are:

1. The emissivity, surface area, and expected temperature of the products of penetration due to meteoroid impact are not precisely determinable from existing knowledge. Estimates of each of these items have been made based upon empirical information. For aluminum walls, the emissivity of penetration products is estimated to be 0.2, and the area is estimated to be equivalent to a spherical surface whose diameter is equal to the diameter of the penetration hole. From these estimates the temperature is estimated to be of the order of 3000 K. for impact velocities of about 7500 feet per second. Aerodynamic heating does not appear to be a significantly contributing factor to the observed signals.

2. The most efficient radiation collecting surface is provided by the surface of the sensor itself. A procedure was developed for determining the optimum position for flat plate sensors in cylindrical tanks. No significant radiation absorption is predicted for transmission to PbS sensors through hydrogen or oxygen. However, for dinitrogen tetroxide absorption may present a limitation to the use of an infrared detection system. For hydrazine, no appreciable absorption is expected. The absorption characteristics of un-symmetrical dimethyl hydrazine (UDMH) are not known.

- 58 -

3.   The use of lead sulfide photoconductive sensors is recommended for a meteoroid penetration detection system from considerations of performance, cost, and system compatibility. For the most difficult detection case that may be assumed for the detection system, the output voltage from a typical PbS sensor would be of the order of 30 microvolts. The required collecting area of the sensor should be approximately 1.0 cm^2. The sensor should have a dark resistance of about 50,000 ohms and have a time constant of about 100 microseconds at room temperature.

4.   The current state of the art permits amplifier designs that are well suited to the requirements of the meteoroid penetration detection system. Such an amplifier should have linear voltage gain of the order of 10,000 for low voltage input signals, with the gain decreasing for higher level input signals to give an output voltage proportional to the logarithm of the input voltage. The amplifier should be transistorized and powered by a DC potential that may be supplied by a battery.

VI SYSTEM DESIGN CRITERIA

The following design criteria are presented on the basis of the experimental and analytical study, for a micrometeoroid penetration detection system that will meet certain anticipated use conditions. These conditions are presented first as a functional specification for the overall system.

Particular design specification limits are subsequently presented for the several sub-systems comprising the overall system.

System Functional Specifications

The functional requirements of the system are to provide electrical output pulses of detectible magnitudes when actuated by radiation resulting from penetrating impacts by micrometeoroids. The radiation source characteristics assumed as the limiting conditions for the system input, and the required output conditions, are detailed below:

Input - A spherical radiation source with the following properties:
  a) Diameter of 0.02 inch
  b) Surface emissivity of 0.2
  c) Average temperature of approximately 3000 K.
  d) Distance to sensor element of at least 10 meters
  e) Essentially dark background
  f) Duration within field of view of sensor, 10^{-4} second

Output - One electrical pulse with the following:
  a) Maximum voltage amplitude within the range of 0.05 v to 5.0 v
  b) Rise time of 0.5 ms or less
  c) Pulse width of 100 microseconds or greater.

Sensor Specifications

The sensor shall be a lead sulfide, photoconductive, plate type sensor with the following characteristics. Performance shall be consistent with the functional requirements of the overall system.

Dimensions   (L $=$ length;   W $=$ width)

Sensitive Area : $0.5 \, cm \leq L \leq 5 \, cm$; $0.5 \, cm \leq W \leq 5 \, cm$

Shall be mountable in a cylindrical mounting of less than two inches in diameter.

Ambient
Temperature   - 253 C. to +50 C.

Resistance   0.03 megohm to 0.10 megohm at 25 C.

Time Constant 50 μ sec to 200 μ sec; at 25 C.

Amplifier Specifications

The amplifier shall be mounted on a printed circuit card. It shall include preamplification, logarithmic gain, and output stages on the same card, and shall be compatible for operation from input signals provided by sensors of the type specified above. Performance shall be consistent with the functional requirements of the overall system, and the following particular specifications shall apply:

Mounted Circuit Card   Dimensions - Length $\leq$ 6 inches, Width $\leq$ 6 inches, Thickness $\leq$ 2 inches

Weight   - $\leq$ 10 ounces.

Gain	For input signals $\leq 10^{-4}$ volt , Linear voltage gain of 10,000 $\pm$ 50 percent
	For input signals $> 10^{-4}$ volt logarithmic voltage gain
	For input signals of 1.0 volt output signal shall be 2.0 to 10.0 volts
Noise	Noise output shall be less than 5 millivolts at 25 C. ambient temperature.
Power Requirement	Less than 1.0 watt at a voltage between 10 and 50 volts, regulated to $\pm$ 10 percent.

APPENDIX A

DETERMINATION OF HOLE SIZE

OF METEOROID PENETRATIONS

This Appendix briefly discusses the problems inherent in the development of an instrumentation system that would provide information for inference of the size of holes formed by penetrating impacts.

From the preceding section on "Theoretical Considerations" there are three physical relationships which govern the radiant energy that is incident on a sensor. The first is the Stefan-Boltzmann Law, which describes the energy emitted by the radiation source, as a function of the temperature, area and emissivity of the source. The second relationship is the inverse square law, which gives the reduction of irradiance with range, assuming no radiation absorption within the tank. Third, the effective irradiance of the sensor will vary as the cosine of the angle of incidence.

It is therefore apparent that if inferences of penetration hole size are to be correlated with the amplitude of infrared sensor signals, corrections must be introduced for range and sensor view angle in order to determine the radiant power emitted by the penetration products which is within the spectral range of the sensor. These range and view angle corrections will be discussed later. However, a more basic problem is to correlate sensor signal with penetration hole size for a constant range and view angle.

Even if one assumes a tank of uniform wall thickness and homogeneous construction, it may be expected that the radiance and spectral distribution of radiation emitted by penetration products may vary with parameters such as:

1. Meteoroid impact velocity
2. Meteoroid mass and composition
3. Angle of impact
4. Composition of fluid within the tank (e.g. liquid or gas, oxidizing or non-oxidizing medium)
5. Material of construction of the wall and its temperature, which affects hole size.

Therefore, it would appear to be rather fortuitous if it should prove to be possible to establish a close empirical correlation between radiance of the penetration products and hole size that would be independent of the above listed variables. In a practical case, the wall construction is likely to be non-uniform in thickness and composition (e.g., internally-ribbed with internal foam insulation for the Saturn S-IV tanks) and therefore the radiance of penetration products is likely to vary with the location of the impact site as well as with the other variables listed above. For these reasons it appears rather unlikely that infrared or visible sensors can be used to give an accurate determination of hole size except under carefully controlled conditions, specifically:

1. With constant wall thickness of a homogeneous material at a known temperature.

2. With a well-defined internal environment such as a vacuum, or a gas of known pressure and composition, or a liquid of known geometrical configuration.

Under such controlled conditions, it may be possible to correlate sensor data to hole size with sufficient accuracy to provide a useful estimate of the hole size or of the initial meteoroid properties. It is apparent that establishment of such a correlation must rely primarily on empirical methods because of the poor state of theoretical understanding of the penetration phenomena and the difficulties and uncertainties inherent in theoretical analysis of the complex processes involved.

It appears probable that a determination of the total radiance of penetration products may not be sufficient to determine hole size or meteoroid properties and that some measure of the effective temperature and emissivity, or of the term $\varepsilon\, T^4$ of the penetration products may also be required in order to determine the effective radiating area of the penetration products which, in turn, could be related to the hole size. In such an event it would be possible to use two or more sensors of differing spectral response characteristics or with different optical bandpass filters to determine the effective temperature of the source (analogous to two-color pyrometry).

It may also prove useful to measure the residual velocity of penetration products and to determine whether such a measurable quantity can be correlated with the radiant properties of penetration products.

Returning now to the problem of corrections to the sensor signal for range and sensor view angle, it is apparent that corrections may be based on measuring

the ratio of the signals from two sensors, both of which measure the amplitude of the radiant pulse from a penetration within their mutual field of view. For example, if two sensors, E and F, are mounted at opposite ends of a cylindrical tank as shown in Figure 21, impacts anywhere at the midplane of the tank would produce equal intensity signals at E and F.

If a penetration occurs at a location P, where the view angles of sensors E and F are θ and $\emptyset$ respectively, the ratio of responses will be:

$$R_{EF} = \frac{\sin^2 \theta \, \cos \theta}{\sin^2 \emptyset \, \cos \emptyset} \tag{1A}$$

For a cylindrical tank of radius R and length L, as shown, the angles θ and $\emptyset$ are related by:

$$\tan \theta = \frac{R}{X} \tag{2A}$$

$$\tan \emptyset = \frac{R}{L - X} \tag{3A}$$

and therefore

$$\tan \emptyset = \frac{R}{\left[L - \dfrac{R}{\tan \theta} \right]} \tag{4A}$$

Expressing $\sin^2 \emptyset$ and $\cos \emptyset$ in terms of θ:

$$\sin^2 \emptyset = \frac{R^2}{\left[L - \dfrac{R}{\tan \theta} \right]^2 + R^2} \tag{5A}$$

- 66 -

$$\cos \theta = \frac{L - \frac{R}{\tan \theta}}{\sqrt{\left[L - \frac{R}{\tan \theta}\right]^2 + R^2}} \tag{6A}$$

Substituting in Equation (1A), the observed signal ratio is related to θ by:

$$R_{EF} = \sin^2 \theta \cos \theta \left(\frac{\left[(L - \frac{R}{\tan \theta})^2 + R^2\right]^{3/2}}{R^2 (L - \frac{R}{\tan \theta})} \right) \tag{7A}$$

A correction factor may be computed and applied to the signal from sensor E to determine a corrected signal equal to the signal which would have been obtained if the penetration had occurred at the midplane, where $\tan \theta_o = \frac{2R}{L}$ the correction factor is:

$$C = \frac{\sin^2 \theta_0 \cos \theta_0}{\sin^2 \theta \cos \theta} \tag{8A}$$

where θ must be determined by computation from Equation (7A), using the experimentally measured signal ratio R_{EF}.

The corrected signal voltage would be a measure of the absolute radiance of the penetration products at the first instant of penetration into the tank, which it is hoped, may be correlated with the puncture size.

Figure 21 presents a schematic block diagram of circuitry that would provide for penetration counting, computation of view angle corrections, determination of the absolute (or spectral) radiance of the penetration products, and computation of penetration hole size. Such a system would count penetrations and determine their size. By extracting the view angle θ, it would also be possible to determine the axial location of the hole, if desired.
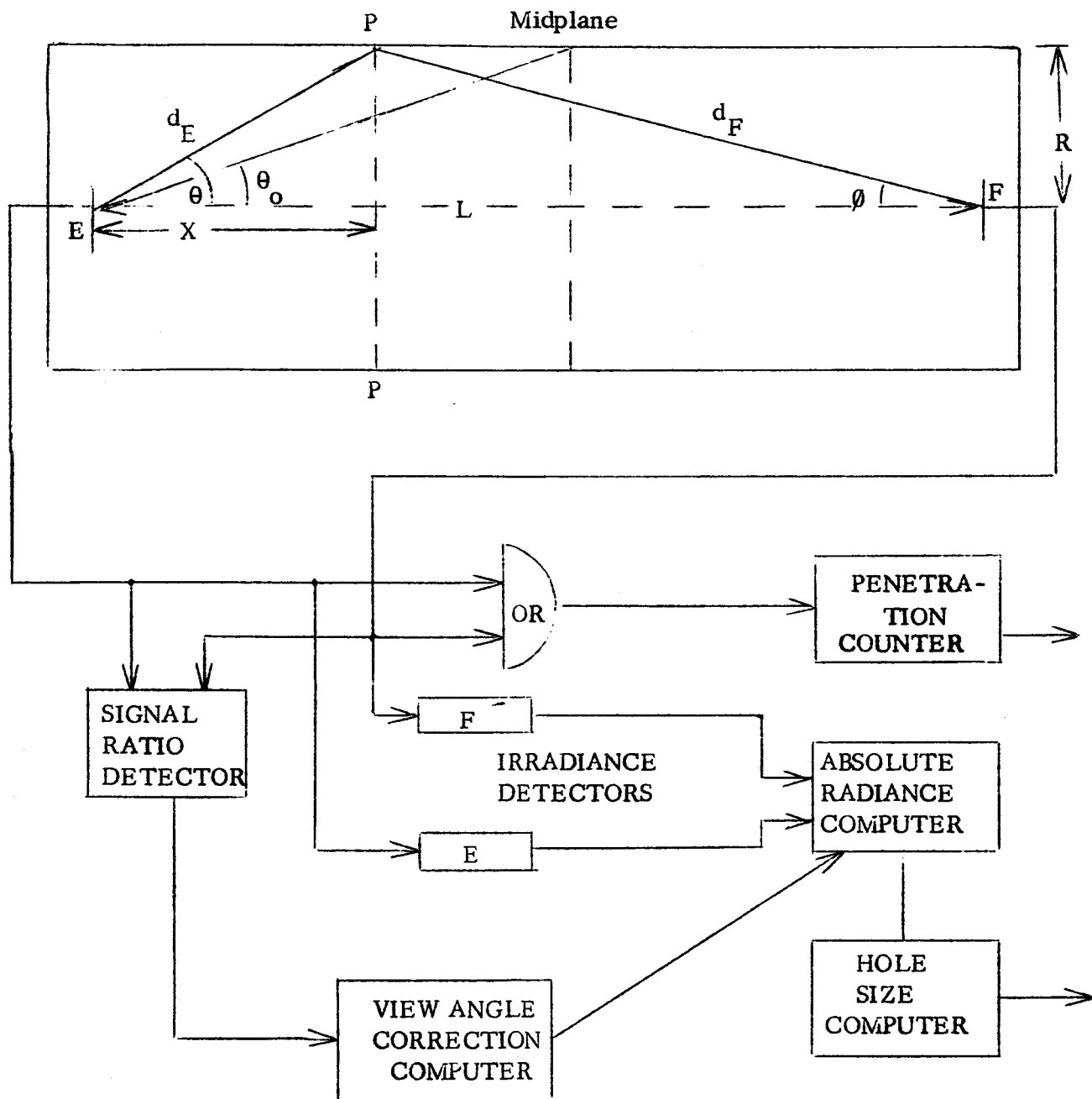
BLOCK DIAGRAM OF HOLE DETECTION SYSTEM

FIGURE 21

REFERENCES

1. Thompson, A.B., and Gell, C.F., "Meteoroids as a Hazard in Space Flight - A Survey of Present Information", American Rocket Society Report No. 2138-61 October, 1961

2. Eichelberger, R.J., and Gehring, J.W., "Effects of Meteoroid Impacts on Space Vehicles", American Rocket Society Report No. 2030-61, October, 1961

3. Bjork, R.L., "Effects of a Meteoroid Impact on Steel and Aluminum in Space", Technical Report, p. 1662, Rand Corporation, Engineering Division, December, 1958.

4. Halperson, S. M., "Observations of Hypervelocity Impact", U.S. Naval Research Laboratory.

5. "Proceedings of the Hypervelocity Techniques Symposium", Institute of the Aeronautical Sciences, October, 1960.

6. Kruse, P.W., McGlaughlin, L.D., and McQuistan, R.B., "Elements of Infrared Technology", John Wiley & Sons, 1962.

7. Personal communication between K. Clark, National Bureau of Standards, and P. G. Luckhardt, Exotech Incorporated, November, 1962.

8. Jakob, M., "Heat Transfer - Volume I", John Wiley & Sons, New York, 1949.

9.   Atkins , W. T., "Flash Associated with High-Velocity Impact on Aluminum", Journal of Applied Physics - Vol. 26, No. 1, pp. 126 - 127, January, 1955.

10.   Personal communications between R. J. Eichelberger, Chief, Detonation Physics Branch, Ballistic Research Laboratories, Aberdeen Proving Ground, Maryland; and W. C. Cooley, Technical Director, Exotech Incorporated.

11.   "Study of Crater Physics", Bi-Monthly Report No. 2, for period ending 19 April 1961. Contract NAS 5-763, Subcontract No. C135A-1043, Space Technology Laboratories, Inc.

12.   Truitt, R.W., "Fundamentals of Aerodynamic Heating", The Ronald Press, New York, 1960.

13.   Allin, E.J., Hare, W.F.J., MacDonald, R.E., "Infrared Absorption of Liquid and Solid Hydrogen", Physical Review, Vol. 98, p. 554, 1955.

14.   Crawford, M.F., Welch, H.L., Locke, J.L., "Infrared Absorption of Oxygen and Nitrogen Induced by Intermolecular Forces", Physical Review, Vol. 75, p. 1607, 1949.

15.   Snyder, R.G., Hisatsune, L.C., "Infrared Spectrum of Dinitrogen Tetroxide", Journal of Molecular Spectroscopy, Vol. 1, p. 139, 1957.

16.   Giguere, P.A., Liu, I.D., "On the Infrared Spectrum of Hydrazine", The Journal of Chemical Physics, Vol. 20, No. 1, p. 136, 1952.

17.   "Infratron Lead Sulfide Photoconductors - A State of the Art Report",
      Infrared Industries Incorporated, Waltham, Mass., 1958.

18.   Texas Instruments, Incorporated - Product Bulletins

19.   Anderson, N.C., "Comparative Performance of Cooled Infrared Photo-
      conductors", Infrared Industries Incorporated, 1958.

20.   Klass, P.J., "Infrared Sensors in Space - Part I", Aviation Week & Space
      Technology, McGraw-Hill Publishing Co., September 24, 1962.

21.   "Radiation Calculator", General Electric Company, Publication: GEM-15-C.